Continued Bcl6 expression prevents the transdifferentiation of established Tfh cells into Th1 cells during acute viral infection

Cell Reports

Article

Continued Bcl6 Expression Prevents the Transdifferentiation of Established Tfh Cells into Th1 Cells during Acute Viral Infection

Graphical Abstract

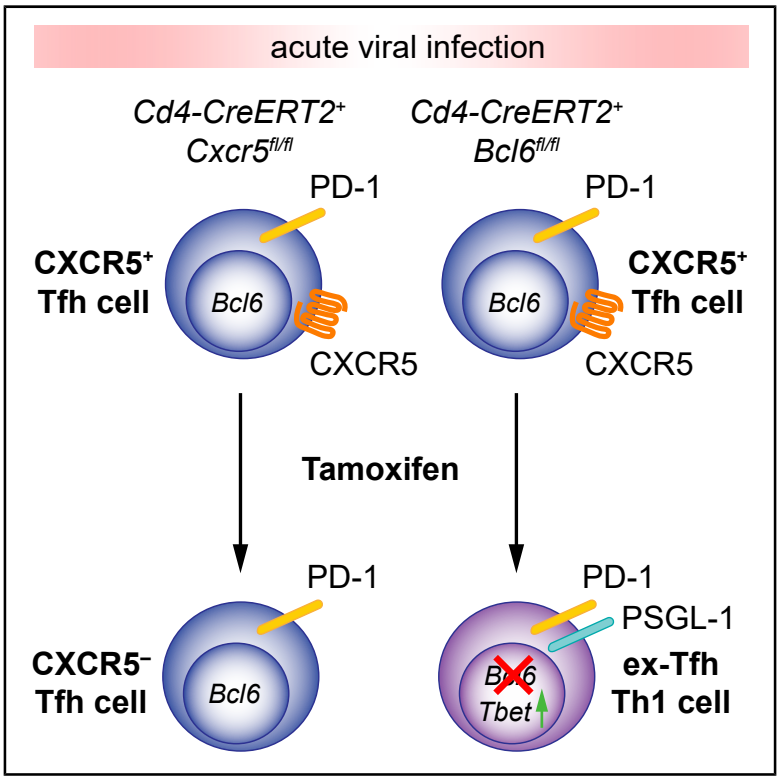

Highlights

- Induced ablation of *Cxcr5* has minor effects on Tfh cell identity and function
- Continued *Bcl6* expression is critical for the maintenance of established Tfh cells
- CD4$^+$ T cell-expressed *Bcl6* is important for the maintenance of germinal centers
- Induced ablation of *Bcl6* converts "ex-Tfh" cells into Th1 cells during LCMV infection

Authors

Dominik Alterauge, Johannes W. Bagnoli, Frank Dahlström, ..., Thorsten Buch, Wolfgang Enard, Dirk Baumjohann

Correspondence

dirk.baumjohann@uni-bonn.de

In Brief

Alterauge et al. show that the induced loss of CXCR5 in established T follicular helper (Tfh) cells has minor effects on Tfh cell identity and germinal center (GC) maintenance. In contrast, induced *Bcl6* ablation in CD4$^+$ T cells results in GC resolution and transdifferentiation of established Tfh cells into Th1 cells during acute viral infection.

Alterauge et al., 2020, Cell Reports *33*, 108232
October 6, 2020
https://doi.org/10.1016/j.celrep.2020.108232

CellPress

Cell Reports

CellPress
OPEN ACCESS

Article

Continued Bcl6 Expression Prevents the Transdifferentiation of Established Tfh Cells into Th1 Cells during Acute Viral Infection

Dominik Alterauge,[1] Johannes W. Bagnoli,[2] Frank Dahlström,[1] Barry M. Bradford,[3] Neil A. Mabbott,[3] Thorsten Buch,[4] Wolfgang Enard,[2] and Dirk Baumjohann[1,5,6,7,*]

[1]Institute for Immunology, Biomedical Center, Faculty of Medicine, LMU Munich, Grosshaderner Str. 9, 82152 Planegg-Martinsried, Germany
[2]Anthropology & Human Genomics, Department of Biology II, LMU Munich, Grosshaderner Str. 2, 82152 Planegg-Martinsried, Germany
[3]The Roslin Institute and the Royal (Dick) School of Veterinary Sciences, University of Edinburgh, Easter Bush, Midlothian EH25 9RG, UK
[4]Institute of Laboratory Animal Science, University of Zurich, Wagistr. 12, 8952 Schlieren, Switzerland
[5]Medical Clinic III for Oncology, Hematology, Immuno-Oncology, and Rheumatology, University Hospital Bonn, University of Bonn, Venusberg-Campus 1, 53127 Bonn, Germany
[6]Twitter: @BaumjohannLab
[7]Lead Contact
*Correspondence: dirk.baumjohann@uni-bonn.de
https://doi.org/10.1016/j.celrep.2020.108232

SUMMARY

T follicular helper (Tfh) cells are crucial for the establishment of germinal centers (GCs) and potent antibody responses. Nevertheless, the T cell-intrinsic factors that are required for the maintenance of already-established Tfh cells and GCs remain largely unknown. Here, we use temporally guided gene ablation in CD4$^+$ T cells to dissect the contributions of the Tfh-associated chemokine receptor CXCR5 and the transcription factor Bcl6. Induced ablation of *Cxcr5* has minor effects on the function of established Tfh cells, and *Cxcr5*-ablated cells still exhibit most of the features of CXCR5$^+$ Tfh cells. In contrast, continued Bcl6 expression is critical to maintain the GC Tfh cell phenotype and also the GC reaction. Importantly, *Bcl6* ablation during acute viral infection results in the transdifferentiation of established Tfh into Th1 cells, thus highlighting the plasticity of Tfh cells. These findings have implications for strategies that boost or restrain Tfh cells and GCs in health and disease.

INTRODUCTION

T follicular helper (Tfh) cells are critically important for providing help to B cells for potent antibody responses (Crotty, 2019; Vinuesa et al., 2016). Tfh cells are characterized by the expression of the chemokine receptor CXCR5 and the transcriptional repressor Bcl6. In addition, they express several co-stimulatory molecules such as inducible T cell co-stimulator (ICOS), CD40L, and B- and T-lymphocyte attenuator (BTLA) and inhibitory receptors such as programmed cell death protein-1 (PD-1) that allow for close interactions with B cells. Furthermore, Tfh cells produce cytokines such as interleukin-4 (IL-4) and IL-21 that instruct B cell class switching and survival.

Tfh cell differentiation is characterized by a multistep differentiation process that involves sequential interactions with dendritic cells (DCs) and B cells in distinct micro-anatomical locations, ultimately leading to the establishment of germinal centers (GCs), in which potent antibodies are generated (Crotty, 2019; Qi, 2016; Vinuesa et al., 2016). The induction of CXCR5- and Bcl6-expressing early Tfh cells from naive CD4$^+$ T cell precursors is mediated by DCs, which at this stage are independent of cognate interactions with B cells (Baumjohann et al., 2011; Goenka et al., 2011). Bcl6 acts as a transcriptional repressor that restricts the expression of inappropriate genes and alternative fates in activated CD4$^+$ T cells, thus promoting Tfh cell differentiation (Hatzi et al., 2015; Johnston et al., 2009; Liu et al., 2016; Nurieva et al., 2009; Yu et al., 2009). While the ensuing migration of these activated CD4$^+$ T cells toward the T-B cell border and follicles is guided by the chemokine receptor CXCR5, simultaneous downregulation of the chemokine receptor CCR7, which is highly expressed on naive T cells, is required to enable activated T cells to re-localize to the T-B zone border and to enter the follicle and GC (Ansel et al., 1999; Arnold et al., 2007; Hardtke et al., 2005; Haynes et al., 2007; Junt et al., 2005). Interestingly, some CXCR5-deficient T helper cells have been observed in B cell areas in some of these studies, while in others they have not. The cause of these contradictory observations remains unclear. Localized within GCs, mature GC Tfh cells express the highest levels of CXCR5 and Bcl6 among CD4$^+$ T cells.

Continued interactions between antigen-presenting cells, in particular B cells, and Tfh cells are required to maintain the Tfh cell phenotype and GC responses (Baumjohann et al., 2013b; Deenick et al., 2010). However, while the T cell-intrinsic factors that are required for the initial steps of Tfh cell differentiation

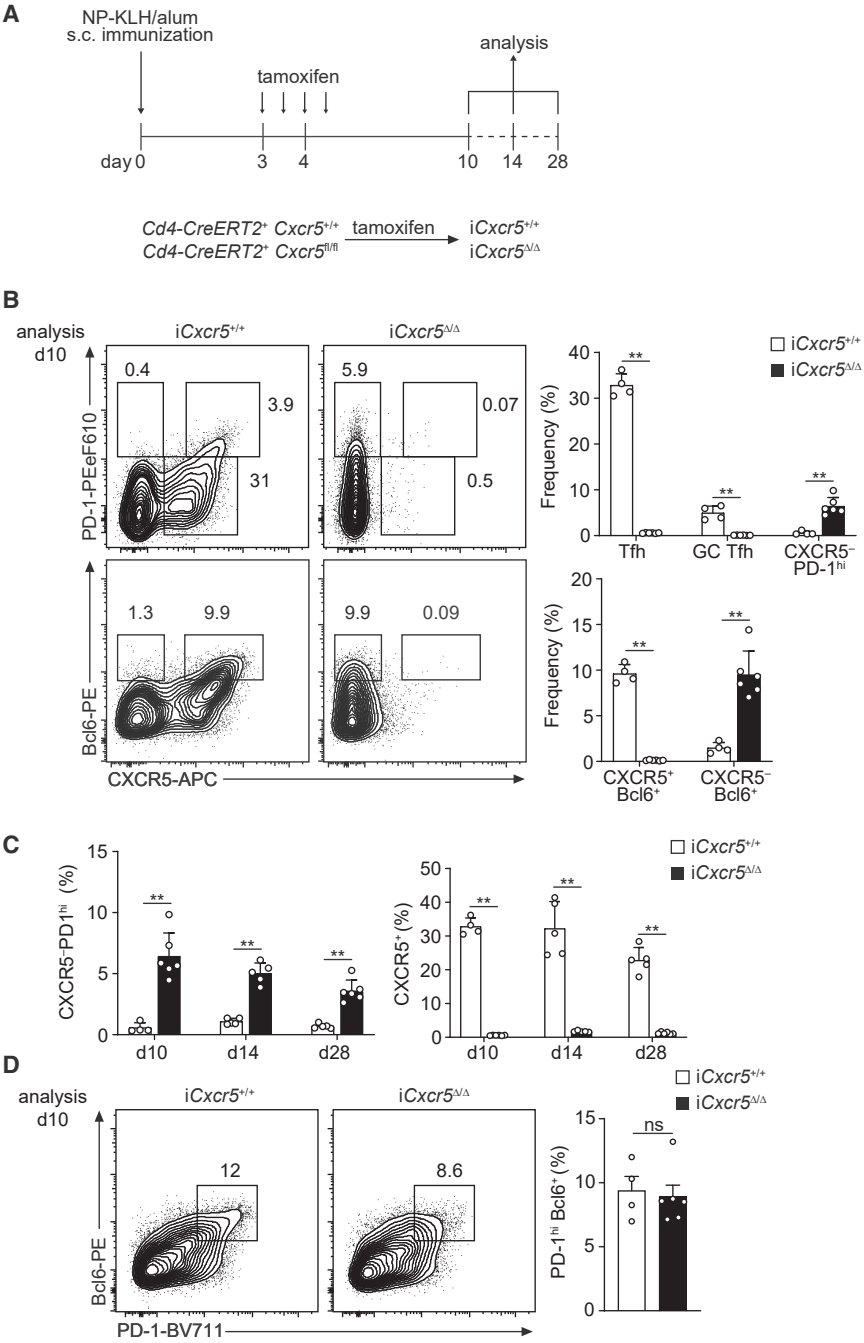

Figure 1. Tfh Cells Continue to Express Tfh Cell Markers upon Induced *Cxcr5* Ablation

(A) Schematic representation of the experimental protocol for the analysis of the impact of induced CD4$^+$ T cell-specific ablation of *Cxcr5* after NP-KLH/alum immunization.

(B) Flow cytometry of CD4$^+$ T cells from draining lymph nodes of tamoxifen-treated *Cd4-CreERT2*$^+$ *Cxcr5*$^{+/+}$ and *Cd4-CreERT2*$^+$ *Cxcr5*$^{fl/fl}$ mice, referred to as i*Cxcr5*$^{+/+}$ and i*Cxcr5*$^{\Delta/\Delta}$, respectively, analyzed on day 10 after immunization. Cells were pre-gated as live CD4$^+$CD44^{hi}CD19$^-$ lymphocytes. Gate frequencies indicate the percentage of CXCR5$^-$PD-1^{hi} cells, CXCR5^{hi}PD-1^{hi} GC Tfh cells, and CXCR5$^+$PD-1$^{lo/int}$ Tfh cells (upper panel) or CXCR5$^-$Bcl6^{hi} cells and CXCR$^+$Bcl6^{hi} GC Tfh cells (lower panel). Right, quantification of the results; each symbol represents an individual mouse (n = 4–6).

(C) Quantification of CXCR5$^-$PD-1^{hi} and CXCR5$^+$ Tfh cells from mice treated as in (B), measured on day 10, 14 and 28 (n = 4–6).

(D) Flow cytometry and quantification of PD-1^{hi}Bcl6^{hi} CD4$^+$ T cells in the draining lymph nodes of mice on day 10 after immunization as in (B) (n = 4–6).

**p < 0.01 two-tailed nonparametric Mann-Whitney test (B–D); means ± SEMs in (B)–(D). See also Figure S1.

have been investigated in more detail (Crotty, 2019; Vinuesa et al., 2016), it remains largely unknown whether and how different T cell-expressed chemokine receptors and transcription factors are also required for the maintenance of already established Tfh cells, in part due to the lack of appropriate experimental systems. Here, we established a system that allowed us to ablate *Cxcr5* and *Bcl6* specifically in CD4$^+$ T cells in a temporally controlled manner to systematically test the requirements of these two factors for Tfh cell and GC maintenance. We found that while CXCR5$^-$ Tfh cells kept most of the Tfh cell features and functions, Bcl6 was strictly required for the maintenance of Tfh cell identity by preventing the transdifferentiation into Th1 cells in an acute viral infection model. These functional insights not only emphasize the high degree of plasticity of Tfh cells but they also give indications about how ongoing GC reactions may be modulated in different disease settings.

RESULTS

Tfh Cells Retain B Cell Helper Capabilities upon Induced *Cxcr5* Ablation

To investigate the impact of a loss of CXCR5 expression in preexisting Tfh cells, we crossed mice bearing an inducible *Cd4-Cre-ERT2* allele to mice containing *loxP*-flanked *Cxcr5* alleles to generate compound mice in which *Cxcr5* can be deleted specifically in CD4$^+$ T cells upon tamoxifen application (designated as i*Cxcr5*$^{\Delta/\Delta}$ mice) (Figure 1A). Tamoxifen application on days 3 and 4 after subcutaneous (s.c.) hock immunization with nitrophenylacetyl conjugated to keyhole limpet hemocyanin (NP-KLH) in alum resulted in an almost complete absence of CXCR5 protein in CD4$^+$ T cells from i*Cxcr5*$^{\Delta/\Delta}$ mice that were analyzed on day 10 after immunization (Figure 1B). i*Cxcr5*$^{+/+}$ mice that

CellPress
OPEN ACCESS

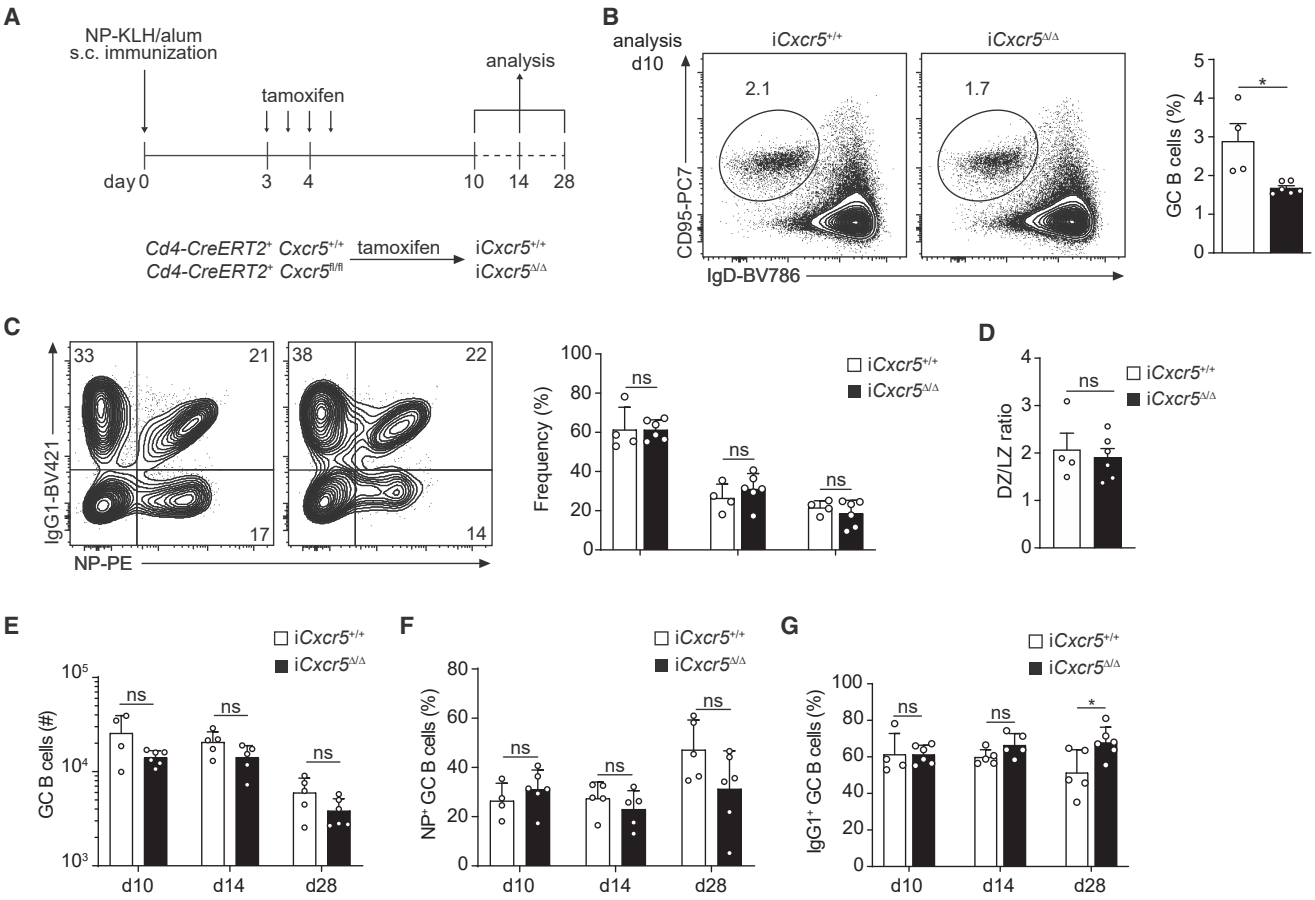

Figure 2. *Cxcr5*-Ablated Tfh Cells Retain B Cell Helper Capabilities

(A) Schematic representation of the experimental protocol for the analysis of the impact of induced CD4$^+$ T cell-specific ablation of *Cxcr5* after NP-KLH/alum immunization.

(B) Flow cytometry of B cells from draining lymph nodes of tamoxifen-treated *Cd4-CreERT2*$^+$ *Cxcr5*$^{+/+}$ and *Cd4-CreERT2*$^+$ *Cxcr5*$^{fl/fl}$ mice, referred to as i*Cxcr5*$^{+/+}$ and i*Cxcr5*$^{\Delta/\Delta}$, respectively, analyzed on day 10 after immunization. Cells were pre-gated as live CD19$^+$CD4$^-$ lymphocytes. Gate frequencies indicate the percentage of IgD^{lo}CD95^{hi} GC B cells. Right, quantification of the results; each symbol represents an individual mouse (n = 4–6).

(C) Flow cytometry and quantification of NP-specific and IgG1$^+$ GC B cells as in (B). the gate frequencies indicate the percentage of IgG1$^+$NP$^-$, IgG1$^+$NP$^+$, and IgG1$^-$NP$^+$ GC B cells.

(D) Ratio of GC B cells with a CXCR4^{hi}CD86^{lo} dark zone (DZ) and CXCR4^{lo}CD86^{hi} light zone (LZ) phenotype in the draining lymph nodes of mice as in (B).

(E–G) Quantification of (E) GC B cell numbers, (F) NP$^+$ GC B cells, and (G) IgG1$^+$ GC B cells from mice as in (B), measured on days 10, 14, and 28 after immunization (n = 4–6).

*p < 0.05, **p < 0.01 two-tailed nonparametric Mann-Whitney test (B–G); means + SEMs in (B)–(G). See also Figure S1.

expressed one allele of *Cd4-CreERT2* but lacked *loxP*-flanked *Cxcr5* alleles served as controls. CXCR5$^+$ PD-1^{int} (Tfh) and CXCR5^{hi}PD-1^{hi} (GC Tfh) cell populations were both absent in i*Cxcr5*$^{\Delta/\Delta}$ mice, further highlighting the very efficient deletion of *Cxcr5* by *Cd4-CreERT2* (Figure 1B). Interestingly, we observed PD-1^{hi} and Bcl6$^+$ cell populations within the CXCR5$^-$ CD4$^+$ T cell compartment in i*Cxcr5*$^{\Delta/\Delta}$ mice that were not present in i*Cxcr5*$^{+/+}$ control mice (Figure 1B). These populations even persisted until days 14 and 28 after immunization without a substantial decrease over time (Figure 1C). The observation that Bcl6 and PD-1 double-positive cells were detectable at similar frequencies in i*Cxcr5*$^{+/+}$ and i*Cxcr5*$^{\Delta/\Delta}$ mice indicated that these CXCR5$^-$ cells retained the expression of Tfh markers associated with GC Tfh cells, with the exception of CXCR5 itself (Figure 1D).

As GC B cells depend strongly on the presence of Tfh cells (Baumjohann et al., 2013b), we additionally assessed the impact of the induced deletion of *Cxcr5* in CD4$^+$ T cells on the B cell response. In i*Cxcr5*$^{\Delta/\Delta}$ mice, the fraction of Fas^{hi}IgD^{lo} GC B cells was reduced compared to i*Cxcr5*$^{+/+}$ control mice on day 10 (Figures 2A and 2B). NP-specific and immunoglobulin G1$^+$ (IgG1$^+$) class-switched GC B cells were not diminished (Figure 2C). Preferential GC B cell localization in the dark zone (DZ) of GCs was also unaffected by the CD4$^+$ T cell-specific *Cxcr5* deletion, as determined by the expression of the DZ and light zone (LZ) markers CXCR4 and CD86, respectively (Figure 2D). GC B cells, IgG1$^+$ class-switched cells, and NP-specific GC B cells were maintained over time until day 28 (Figures 2E–2G). Interestingly, we observed a trend toward a higher abundance of class-switched IgG1$^+$ cells throughout the immune response, which

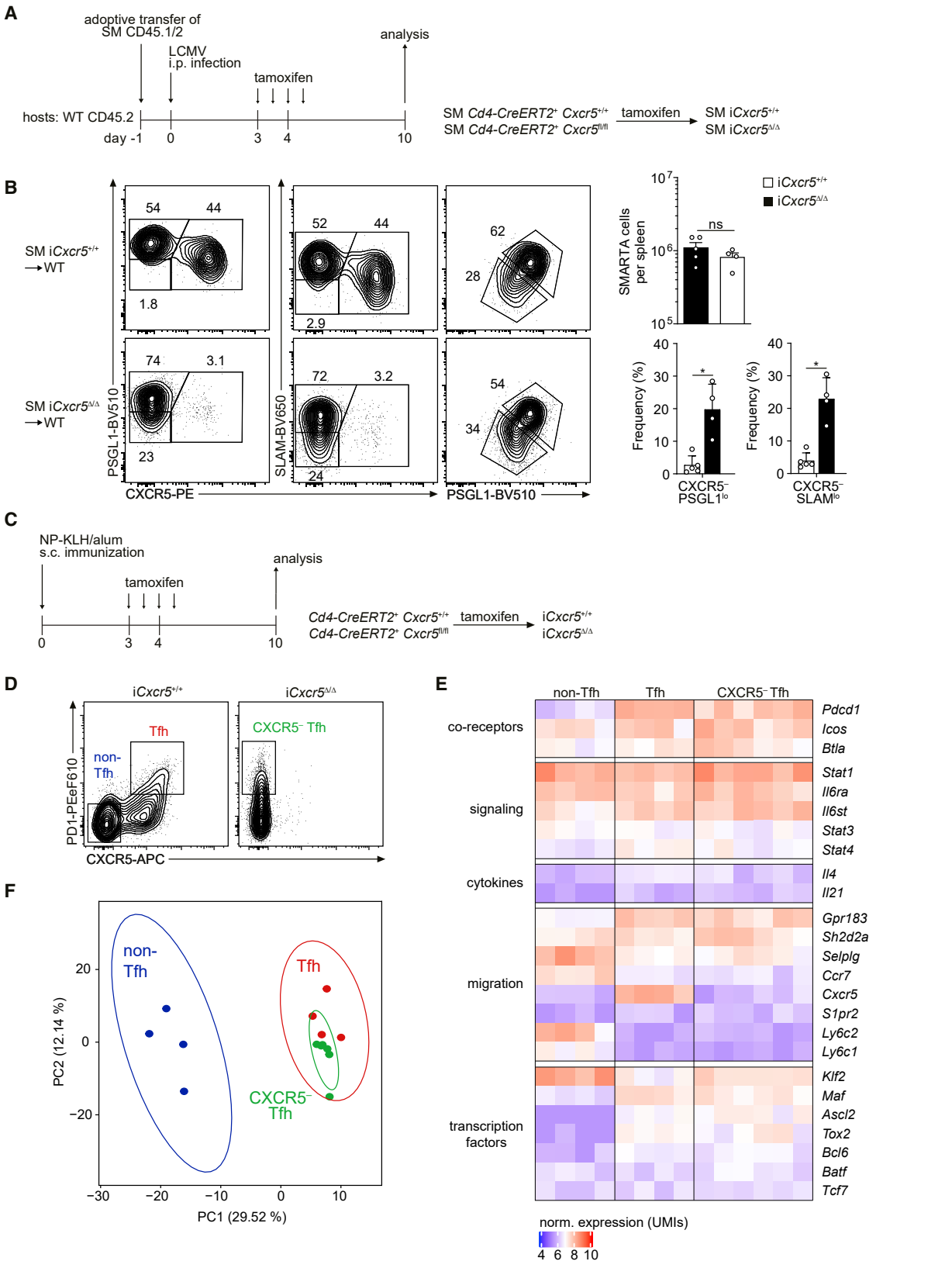

(legend on next page)

became more prominent by day 28 (Figure 2G). These findings demonstrated that certain aspects of the GC response did not depend on the continued presence of CXCR5 on the surface of CD4$^+$ T cells. When *Cxcr5* ablation was induced at the peak of the GC reaction on days 6 and 7 after immunization, similar effects on the maintenance of Tfh cell marker expression and GC B cell helper capabilities were observed (Figure S1).

Induced *Cxcr5* Deficiency Has Little Impact on the Identity of Tfh Cells

To further explore the consequences of *Cxcr5* ablation on established Tfh cells, we next crossed the *Cd4-CreERT2*$^+$*Cxcr5*$^{+/+}$ and *Cd4-CreERT2*$^+$*Cxcr5*$^{fl/fl}$ mice to animals bearing the lymphocytic choriomeningitis virus (LCMV)-specific SMARTA (SM) T cell receptor (TCR) transgene and congenic *Cd45* alleles. Naive CD4$^+$ T cells from these mice were adoptively transferred into wild-type hosts, followed by intraperitoneal (i.p.) infection with LCMV Armstrong to induce an acute viral infection (Figure 3A). Tamoxifen was administered on days 3 and 4 and the phenotype of the transferred SM cells was analyzed by flow cytometry on day 10. In agreement with our findings from the immunization experiments, we observed a population of CXCR5$^-$ i*Cxcr5*$^{\Delta/\Delta}$ SM cells that exhibited surface marker expression reminiscent of Tfh cells with low levels of P-selectin glycoprotein ligand-1 (PSGL-1) and signaling lymphocytic activation molecule (SLAM) (Figure 3B). To examine whether CXCR5-deficient Tfh cells only kept a few Tfh cell markers or maintained an overall Tfh-characteristic expression profile, we conducted RNA sequencing (RNA-seq) of CD4$^+$ T cells after subcutaneous NP-KLH/alum immunization (Figure 3C). C*xcr5* ablation was induced by tamoxifen gavage on days 3 and 4. On day 10 after immunization, CXCR5$^-$ Tfh (CD44^{hi}CXCR5$^-$PD-1^{hi}GITR^{lo}) cells were sorted from i*Cxcr5*$^{\Delta/\Delta}$ mice together with Tfh (CD44^{hi}CXCR5$^+$PD-1^{hi}GITR^{lo}) and non-Tfh (CD44^{hi}CXCR5$^-$PD-1^{lo}GITR^{lo}) cells from control i*Cxcr5*$^{+/+}$ mice (Figure 3D). Sorted cells were pre-gated on GITR^{lo} cells to avoid contamination with regulatory T (Treg) cells, which may also express PD-1. This strategy also excluded T follicular regulatory (Tfr) cells. Transcriptomic analysis revealed that the expression profile of CXCR5$^-$ Tfh cells exhibited an extensive overlap with the profile of CXCR5$^+$ Tfh cells, thereby remaining clearly distinct from non-Tfh cells (Figure 3E). Similar to their *Cxcr5*-sufficient Tfh cell counterparts, CXCR5$^-$ Tfh cells showed characteristic expression patterns of co-receptors (high *Pdcd1* and *Icos*), signaling molecules (high *Il6st*), migratory molecules (high *Sh2d2a*; low *Selplg*, *Ccr7*, and *Ly6c2*), and transcription factors (increased *Maf*, *Tox2*, and *Ascl2*; decreased *Klf2*) (Figure 3E). Principal-component analysis (PCA) using the 500 most variable genes confirmed that the PD-1^{hi} cells from i*Cxcr5*$^{\Delta/\Delta}$ mice were transcriptionally similar to *Cxcr5*-sufficient Tfh cells and differed strongly from non-Tfh cells (Figure 3F). More important, we could corroborate the largely unaltered identity of CXCR5$^-$ Tfh cells also in our SM-based adoptive transfer model, in which i*Cxcr5*$^{\Delta/\Delta}$ SM Tfh cells clearly shared a transcriptomic signature similar to i*Cxcr5*$^{+/+}$ SM Tfh cells (data not shown). Likewise, the transcriptomic signature of i*Cxcr5*$^{\Delta/\Delta}$ SM Th1 cells tightly overlapped with that of i*Cxcr5*$^{+/+}$ SM Th1 control cells (data not shown). In summary, these data showed that the transcriptional programming of established Tfh cells did not depend on continued expression of *Cxcr5*.

Continued T Cell-Specific *Bcl6* Expression Is Critical for GC Tfh and GC B Cell Maintenance

As we could show that the Tfh cell hallmark chemokine receptor CXCR5, which historically helped to define the term "Tfh cells" (Ansel et al., 1999; Breitfeld et al., 2000; Schaerli et al., 2000), was not required for the maintenance of the Tfh cell phenotype, we next investigated the requirement of the Tfh cell master regulator Bcl6 using our inducible-knockout system. To this end, *Bcl6*$^{fl/fl}$ mice, which allow for the deletion of the Bcl6 DNA-binding domain, were intercrossed with the aforementioned *Cd4-CreERT2* strain. Efficient tamoxifen-induced deletion of *Bcl6* was confirmed on the genomic DNA and mRNA levels (Figures S2A and S2B). We then analyzed the impact of tamoxifen-induced, CD4$^+$ T cell-specific *Bcl6* ablation on the T and B cell response after subcutaneous NP-KLH immunization (Figure 4A). We chose two different time points of *Bcl6* ablation when Tfh cells were either already formed early on during the immune response (tamoxifen gavage on days 3 and 4) or later when the GC response was full blown (days 6 and 7). We observed a reduction in the frequency of CXCR5$^+$ PD-1$^{int/lo}$ (Tfh) CD4$^+$ T cells after *Bcl6* ablation, which was more pronounced for the early tamoxifen time point (Figures 4B and S2C). There was also a significant decrease in the frequency of CXCR5^{hi}PD-1^{hi} GC Tfh cells in i*Bcl6*$^{\Delta/\Delta}$ mice as compared to control i*Bcl6*$^{+/+}$ mice for both ablation time points (Figures 4B and S2C). In line with the lower expression

Figure 3. Induced *Cxcr5* Deficiency Has Little Impact on the Identity of Tfh Cells

(A) Schematic representation of the experimental protocol for the analysis of the impact of induced CD4$^+$ T cell-specific ablation of *Cxcr5* in SMARTA (SM) cells after i.p. infection with LCMV Armstrong.

(B) Flow cytometry of splenocytes from tamoxifen-treated wild-type recipient mice that had received adoptively transferred naive *Cd4-CreERT2*$^+$ *Cxcr5*$^{+/+}$ SM and *Cd4-CreERT2*$^+$ *Cxcr5*$^{fl/fl}$ SM cells, followed by i.p. infection of recipients with LCMV Armstrong and analysis 10 days later. Pre-gated as live CD4$^+$CD45.1/2CD19$^-$ lymphocytes. The gate frequencies indicate the percentage of CXCR5$^-$PSGL-1^{lo} or CXCR5$^-$SLAM^{lo} cells, CXCR5$^-$PSGL-1^{hi}, CXCR5$^-$SLAM^{hi}, or PSGL-1^{hi}SLAM^{hi} Th1 cells and CXCR5$^+$ or PSGL-1^{lo}SLAM^{lo} Tfh cells. Right, quantification of the results; each symbol represents an individual mouse (n = 4–5).

(C) Schematic representation of the experimental protocol for the analysis of the impact of induced CD4$^+$ T cell-specific ablation of *Cxcr5* after NP-KLH/alum immunization.

(D) Non-Tfh (CXCR5$^-$PD-1$^-$GITR^{lo}, n = 4) and Tfh cells (CXCR5$^+$PD-1^{hi}GITR^{lo}, n = 4) from i*Cxcr5*$^{+/+}$ mice and CXCR5$^-$ Tfh cells (CXCR5$^-$PD-1^{hi}GITR^{lo}, n = 6) from i*Cxcr5*$^{\Delta/\Delta}$ mice were sorted on day 10 after immunization for RNA-seq. Pre-gated as live CD4$^+$CD19$^-$ lymphocytes.

(E) Heatmap of the normalized expression of selected Th1 or Tfh genes (rows) in non-Tfh, Tfh, and CXCR5$^-$ Tfh cells (columns) sorted as in (D).

(F) Principal-component analysis (PCA) of non-Tfh, Tfh, and CXCR5$^-$ Tfh cell transcriptomes obtained from samples sorted as in (D). Ellipses surrounding the data points delineate computed confidence ellipses with a 95% confidence level.

*p < 0.05, **p < 0.01 two-tailed nonparametric Mann-Whitney test (B); means ± SEMs in (B).

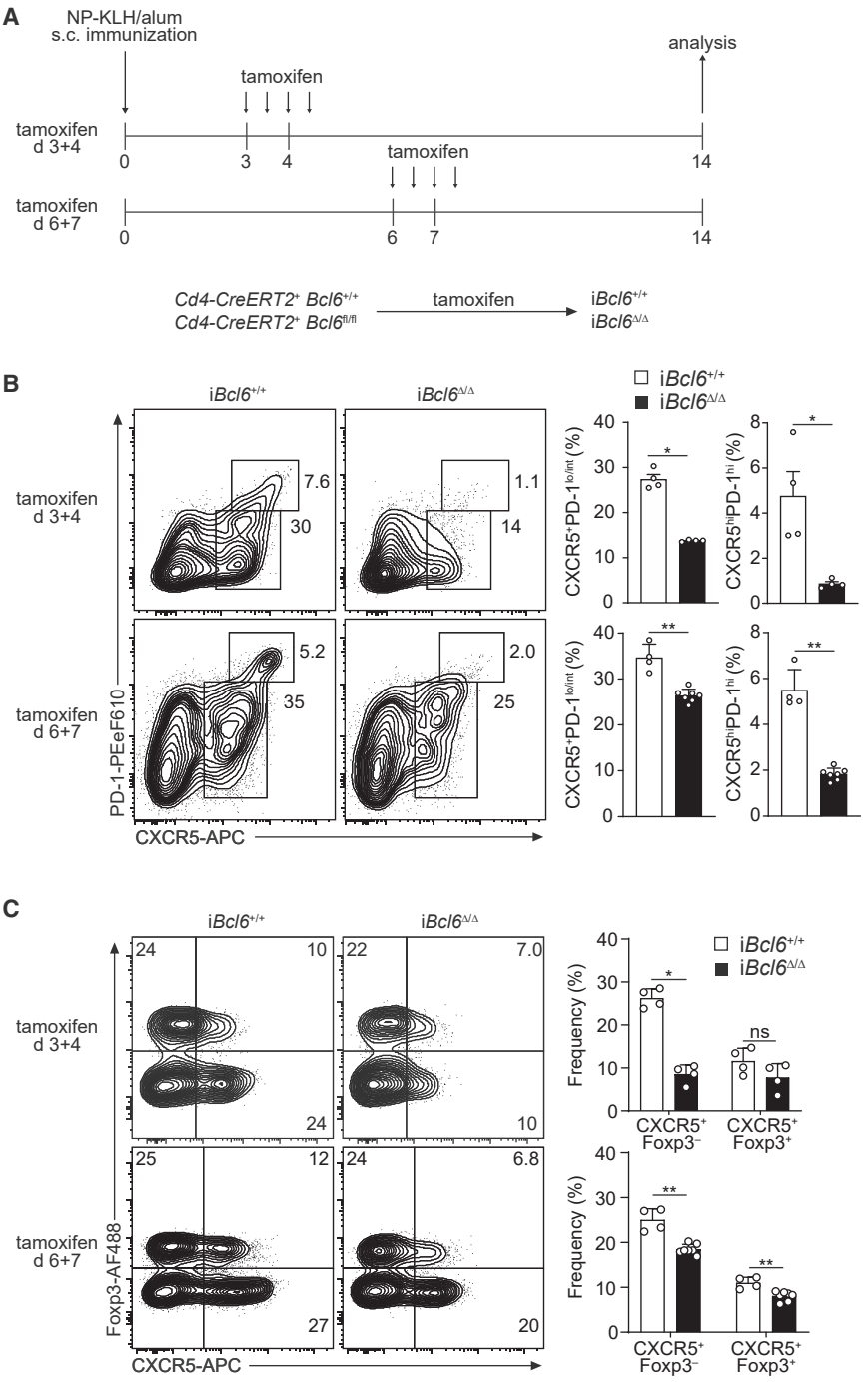

Figure 4. Continued T Cell-Specific *Bcl6* Expression Is Required for GC Tfh Cell Maintenance

(A) Schematic representation of the experimental protocol for the analysis of the impact of induced $CD4^+$ T cell-specific ablation of *Bcl6* at 2 different time points after s.c. hock immunization with NP-KLH/alum.

(B) Flow cytometry and quantification of $CXCR5^+PD\text{-}1^{lo/int}$ Tfh cells and $CXCR5^{hi}PD\text{-}1^{hi}$ GC Tfh cells from the draining lymph nodes of mice treated with tamoxifen on days 3 and 4 (upper panel) or days 6 and 7 (lower panel) and analyzed on day 14 after immunization, pre-gated as live $CD4^+CD44^{hi}CD19^-$ lymphocytes. Right, quantification of the results; each symbol represents an individual mouse (n = 4–7).

(C) Flow cytometry and quantification of Tfh and Tfr cells in the draining lymph nodes of mice as in (B), pre-gated as live $CD4^+CD44^{hi}CD19^-$ lymphocytes. The gate frequencies indicate the percentage of $CXCR5^-Foxp3^+$ Treg cells, $CXCR5^+Foxp3^+$ Tfr cells, and $CXCR5^+Foxp3^-$ Tfh cells.

*p < 0.05, **p < 0.01 two-tailed nonparametric Mann-Whitney test (B and C); means ± SEMs in (B) and (C). See also Figure S2.

of PD-1 and CXCR5, induced *Bcl6* deficiency also resulted in a reduction of $PSGL\text{-}1^{lo}$ cells that are normally representative of GC Tfh cells (Figures S2D and S2E). Interestingly, when tamoxifen was administered on the earlier time point (days 3 and 4), $CXCR5^+Foxp3^+$ Tfr cell frequencies were almost unchanged, while $CXCR5^+Foxp3^-$ Tfh cells were strongly diminished, resulting in an altered Tfh:Tfr ratio (Figure 4C).

The induced loss of *Bcl6* had a strong impact on the GC B cell response. The frequencies of GC B cells were significantly decreased in immunized $iBcl6^{\Delta/\Delta}$ mice as compared to control mice (Figures 5A and 5B). Similar to the stronger reduction of Tfh cells that we observed for days 3 and 4 versus days 6 and 7 tamoxifen treatment, *Bcl6* ablation on days 3 and 4 caused a more pronounced decrease in GC B cell frequencies than tamoxifen gavage on days 6 and 7 (Figure 5B). While the total pool of antigen-specific NP^+ GC B cells was not affected in $iBcl6^{\Delta/\Delta}$ mice in both settings, we observed a defect in class switching toward IgG1 in the days 3 and 4 tamoxifen administration setting (Figure 5C). Consequently, the generation of $IgG1^+NP^+$ cells was also impaired in $iBcl6^{\Delta/\Delta}$ mice with an ~2.5-fold frequency decrease as compared to the control group (Figure 5C). In contrast, T cell-specific *Bcl6* ablation at the peak of the GC reaction (days 6 and 7 after immunization) did not cause obvious alterations in class switching and NP specificity (Figure 5C). The established GC Tfh cells were particularly sensitive to the induced loss of *Bcl6* expression, which also impeded the maintenance of GC B cell frequencies.

Induced *Bcl6* Ablation Alters the Ratio of Tfh versus Th1 Cells during Acute Viral Infection

The data from the previous immunization experiments indicated that Bcl6 expression was particularly vital for GC Tfh cells. To gain further insight into the role of Bcl6 for Tfh cell maintenance,

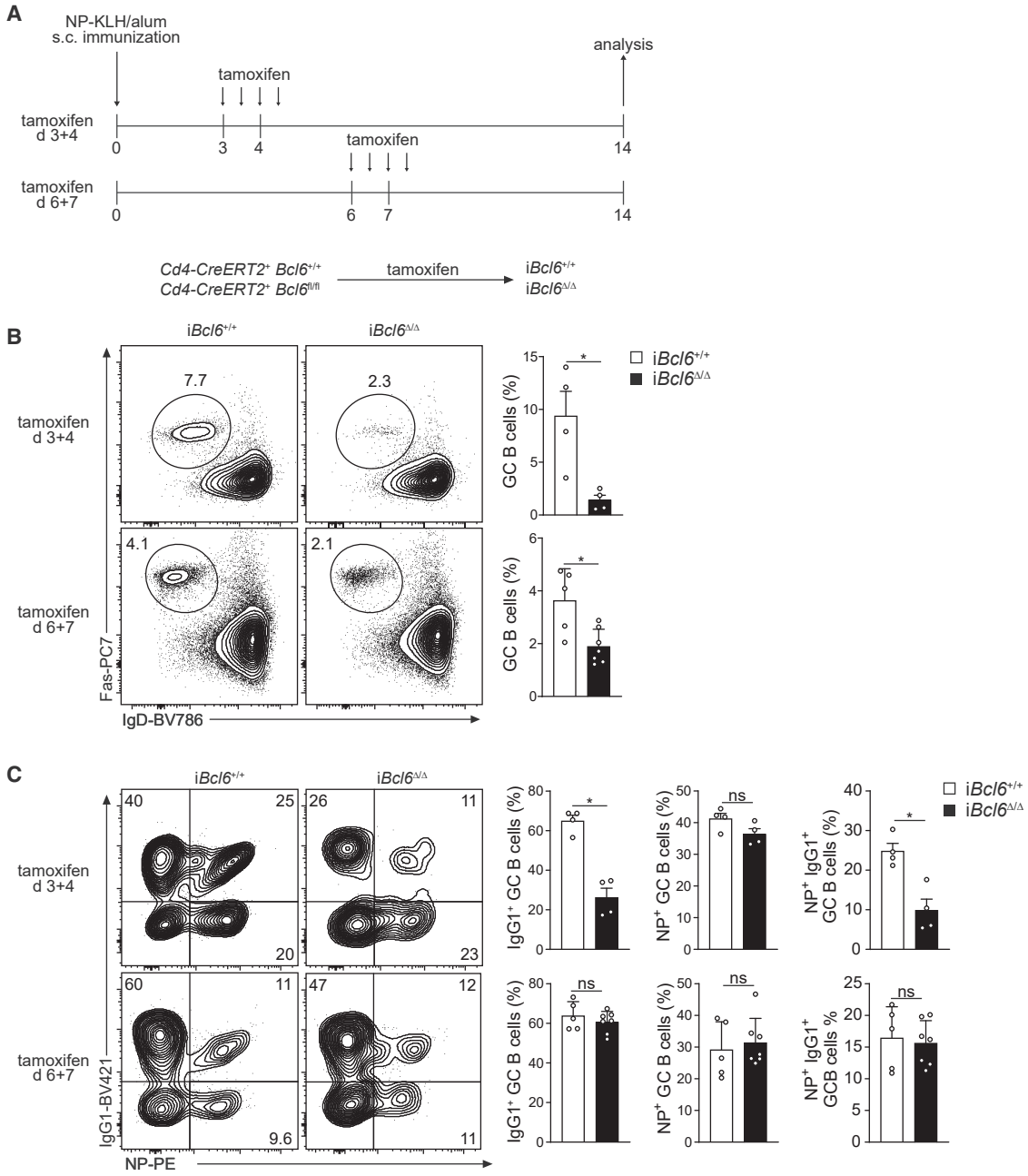

Figure 5. GC B Cell Responses Are Impaired upon the Induced Loss of *Bcl6* in CD4$^+$ T Cells

(A) Schematic representation of the experimental protocol for the analysis of the impact of induced CD4$^+$ T cell-specific ablation of *Bcl6* at 2 different time points after s.c. hock immunization with NP-KLH/alum.

(B) Flow cytometry and quantification of IgD^{lo}CD95^{hi} GC B cells in the draining lymph nodes of mice treated with tamoxifen on days 3 and 4 (upper panel) or days 6 and 7 (lower panel) and analyzed on day 14 after immunization, pre-gated as live CD19$^+$CD4$^-$ lymphocytes. Right, quantification of the results; each symbol represents an individual mouse (n = 4–7).

(C) Flow cytometry and quantification of NP-specific and IgG1$^+$ GC B cells as in (B). The gate frequencies indicate the percentage of IgG1$^+$NP$^-$, IgG1$^+$NP$^+$, and IgG1$^-$NP$^+$ GC B cells.

*p < 0.05, **p < 0.01 two-tailed nonparametric Mann-Whitney test (B and C); means ± SEMs in (B) and (C).

we conducted cell fate analyses. In contrast to induced *Cxcr5* deletion, *Bcl6*-ablated CD4$^+$ T cells did not exhibit continued Tfh cell marker expression, thus hampering the tracking of these cells. To circumvent this issue, we used congenically marked SM cells of *Cd4-CreERT2*$^+$*Bcl6*$^{+/+}$ and *Cd4-CreERT2*$^+$*Bcl6*$^{fl/fl}$ genetic backgrounds to follow the fate of these LCMV-specific

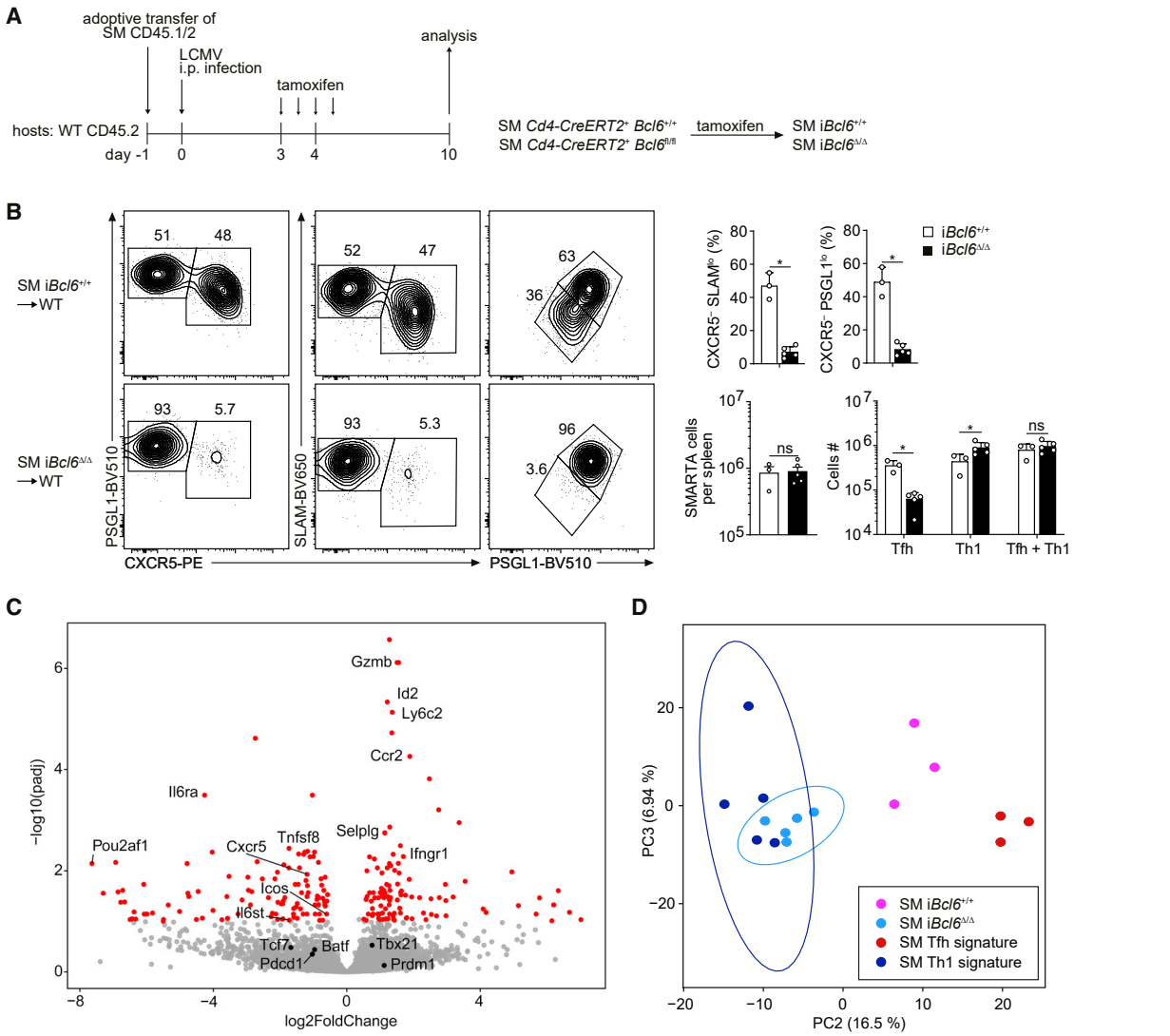

Figure 6. Induced *Bcl6* Ablation Alters the Ratio of Tfh versus Th1 Cells during Acute Viral Infection

(A) Schematic representation of the experimental protocol for the analysis of the impact of induced CD4$^+$ T cell-specific ablation of *Bcl6* in SM cells after LCMV Armstrong infection.

(B) Flow cytometry of splenocytes from tamoxifen-treated wild-type recipients that had received adoptively transferred naive *Cd4-CreERT2*$^+$ *Bcl6*$^{+/+}$ SM and *Cd4-CreERT2*$^+$ *Bcl6*$^{fl/fl}$ SM cells, followed by i.p. infection of recipients with LCMV Armstrong and analysis 10 days later. Pre-gated as live CD4$^+$CD45.1/2CD19$^-$ lymphocytes. The gate frequencies indicate the percentage of CXCR5$^-$PSGL-1^{hi}, CXCR5$^-$SLAM^{hi}, or PSGL-1^{hi}SLAM^{hi} Th1 cells and CXCR5$^+$ or PSGL-1^{lo}SLAM^{lo} Tfh cells. Right, quantification of the results; each symbol represents an individual mouse (n = 3–5).

(C) Volcano plot of differentially expressed genes between i*Bcl6*$^{+/+}$ SM and i*Bcl6*$^{\Delta/\Delta}$ SM cells. The relevant genes are indicated. The red dots depict significantly up- or downregulated genes (adjusted $p < 0.1$, fold change ≥ 0.5).

(D) PCA analysis of i*Bcl6*$^{+/+}$ SM and i*Bcl6*$^{\Delta/\Delta}$ SM cell transcriptomes and signatures of SM i*Cxcr5*$^{+/+}$ Th1 and Tfh cells from 2 independently performed experiments. Each dot represents donor cells from individual recipient mice. The ellipses surrounding the data points delineate computed confidence ellipses with a 95% confidence level.

*$p < 0.05$, **$p < 0.01$ two-tailed nonparametric Mann-Whitney test (B); means ± SEMs in (B).

CD4$^+$ T cells after transfer into wild-type mice, followed by LCMV Armstrong infection on day 0 and tamoxifen treatment on days 3 and 4 to ablate *Bcl6* (Figure 6A). By day 10 after infection, control i*Bcl6*$^{+/+}$ SM cells had differentiated roughly equally into Th1 and Tfh cell populations (Figure 6B). Induced *Bcl6* deficiency resulted in an almost complete loss of CXCR5$^+$ cells and a concomitant increase in Th1 cell frequencies, while the total number of SM cells per spleen remained unaltered (Figure 6B). Low SLAM and PSGL-1 expression levels, which are normally associated with Tfh cells, were not maintained in the absence of *Bcl6* (Figure 6B). Instead, *Bcl6*-ablated cells appeared to have regained the expression of both markers. In fact, the decrease in Tfh cell numbers was paralleled by an increase in Th1 cell numbers (Figure 6B). Since total i*Bcl6*$^{\Delta/\Delta}$ SM cell numbers were not changed,

this suggested that Th1 cells either compensated for the loss of Tfh cells through increased proliferation or that *Bcl6*-ablated "ex-Tfh" cells had adopted a Th1 cell phenotype.

Bcl6 Prevents the Transdifferentiation of Tfh Cells into Th1 Cells during Acute Viral Infection

To dissect whether i*Bcl6*$^{\Delta/\Delta}$ ex-Tfh SM cells converted into bona fide Th1 cells or still exhibited a Tfh-like transcriptional program in the background, we sorted CD45.1/2^{+} i*Bcl6*$^{+/+}$ and i*Bcl6*$^{\Delta/\Delta}$ SM cells for RNA-seq and transcriptomic analyses. Significant changes in differentially expressed genes between i*Bcl6*$^{+/+}$ and i*Bcl6*$^{\Delta/\Delta}$ SM cells revealed many Th1-associated genes being upregulated in i*Bcl6*$^{\Delta/\Delta}$ SM cells (e.g., *GzmB*, *Id2*, *Ifngr1*, *Ly6c2*) (Figure 6C). In contrast, numerous important Tfh cell molecules, including *Cxcr5*, *Il6ra*, *Il6st*, and *Pou2af1* were downregulated. To assess the similarity of the SM i*Bcl6*$^{\Delta/\Delta}$ cells to Th1 cell transcriptomes (Figure 6D), we used Th1 and Tfh signatures of SM i*Cxcr5*$^{+/+}$ control cells obtained from a complementary adoptive transfer experiment (data not shown). Here, we used PC2 and PC3, since most of the variability represented by the first principal component was due to batch effects, which is commonly observed when independently generated RNA-seq data are compared. The control Th1 and Tfh signatures were separated and the transcriptomes of *Bcl6*-sufficient SM cells were found in between them (Figure 6D), as the cells consisted of an equal mixture of Th1 and Tfh cells (Figure 6B). The biological replicates of *Bcl6*-ablated SM cells clustered closely with the Th1 transcriptomes (Figure 6D). This indicated that these cells did not maintain a Tfh cell transcriptional pattern but instead had adopted a Th1 cell gene expression program. This supported our initial hypothesis that the induced loss of Bcl6 in Tfh cells led to transdifferentiation into Th1 cells. To finally prove this *in vivo*, we conducted a retransfer experiment to also exclude the possibility that *Bcl6*-ablated cells were lost during the immune response and were compensated for by increased Th1 cell expansion. To this end, we first co-transferred CD45.1/2 *Cd4-CreERT2*$^{+}$*Bcl6*$^{+/+}$ and CD45.1/1 *Cd4-CreERT2*$^{+}$*Bcl6*$^{fl/fl}$ SM cells into primary hosts, followed by acute LCMV Armstrong infection (Figure 7A). Four days later, Th1 (CXCR5^{-}PSGL-1^{hi}) and Tfh (CXCR5^{+}PSGL-1^{lo}) cells from both genotypes were retransferred into infection-matched secondary hosts (Figure 7B). *Bcl6* was then deleted in the retransferred i*Bcl6*$^{\Delta/\Delta}$ SM cells with tamoxifen on days 5 and 6 after infection. i*Bcl6*$^{+/+}$ SM cells served as controls. The phenotypic stability of the transferred Th1 and Tfh SM cells was assessed on day 12 post-infection by flow cytometry and revealed that Th1 cells maintained the CXCR5^{-}PSGL-1^{hi}SLAM^{lo} Th1 cell identity regardless of *Bcl6* ablation (Figures 7B and 7C). The majority of the transferred i*Bcl6*$^{+/+}$ control SM Tfh cells continued to display a Tfh phenotype, while ~30% downregulated CXCR5 and gained PSGL-1 expression reminiscent of Th1 cells. In contrast, the ability of SM Tfh cells, which had been rendered *Bcl6* deficient (i*Bcl6*$^{\Delta/\Delta}$), to gain Th1 cell marker expression was strongly increased from ~20% to >70% (Figures 7B and 7C). Nevertheless, the total number of SM cells per spleen was unaffected by the induced *Bcl6* knockout (Figure 7D). Moreover, *Bcl6*-ablated cells also expressed higher levels of the Th1-associated transcription factor T-bet compared to the *Bcl6*-sufficient SM control cells (Figure 7E). These data demonstrated that the loss of *Bcl6* in established Tfh cells resulted in a phenotypical shift toward Th1 surface marker expression, which was underlined by the adoption of a Th1-like transcriptional program.

DISCUSSION

Tfh cell differentiation is a multistep process that involves sequential cognate interactions with DCs and B cells in different micro-anatomical locations within secondary lymphoid organs (Crotty, 2019; Qi, 2016; Vinuesa et al., 2016). These processes are highly regulated on the molecular level by various transcription factors and microRNAs (miRNAs) (Maul et al., 2019; Qin et al., 2018). Until recently, it was difficult to assess the requirements of T cell-intrinsic factors that are required for the maintenance of already established Tfh cells. Here, we used temporally guided ablation of the Tfh cell characteristic genes *Cxcr5* and *Bcl6* to systematically assess their requirements for Tfh cell maintenance. Ablation of *Cxcr5* in preexisting Tfh cells showed minor effects on the identity of these cells and their B cell helper abilities. In contrast, continued *Bcl6* expression in T cells was critical for the maintenance of GC Tfh and GC B cells. More important, our data highlighted Bcl6 as a gatekeeper of Tfh cell plasticity *in vivo* that limited the transdifferentiation of established Tfh cells into Th1 cells during acute viral infection.

Several studies have addressed the requirement of CXCR5 expression by Tfh cells for entering the follicle and induction of GCs (Ansel et al., 1999; Arnold et al., 2007; Hardtke et al., 2005; Haynes et al., 2007; Junt et al., 2005). CXCR5-deficient CD4^{+} T cells could still mount GC B cell responses, although the size of GCs was reduced and the frequencies of GC B cells and class switching were slightly lower (Arnold et al., 2007; Haynes et al., 2007). It should be noted that CXCR5-dependent follicular recruitment may also be bypassed by some T helper cells that are passively dragged into the follicle by B cells (Okada et al., 2005). Interestingly, mice that lack CXCR5^{+} CD4^{+} T cells were completely resistant to collagen-induced arthritis, despite grossly normal GC formation (Moschovakis et al., 2017). Previously, it was difficult to assess the role of CXCR5, especially during later stages of the GC response due to the lack of conditional *Cxcr5* alleles. Instead, these studies relied either on adoptively transferred TCR-tg cells or mixed bone marrow chimeras using CXCR5$^{-/-}$ backgrounds. We therefore devised a versatile *in vivo* system that allowed us to delete a gene of interest specifically in CD4^{+} T cells in a temporally controlled fashion. Using this system, we explored the effect of acute ablation of *Cxcr5* in settings of polyclonal as well as antigen-specific TCR-tg CD4^{+} T cell responses, with an emphasis on already-established Tfh cells. Interestingly, Tfh cells that no longer expressed CXCR5 on their surface were able to sustain the high, Tfh-characteristic protein expression levels of PD-1 and Bcl6. In addition, the transcriptome of *Cxcr5*-ablated cells was very similar to that of the *Cxcr5*-sufficient control cells. These findings emphasize that CD4^{+} T cells can not only circumvent the need of CXCR5 expression for GC localization (Moriyama et al., 2014) but they also do not require continued CXCR5 expression to maintain their phenotype. This is surprising, as GC-localized Tfh cells express the highest levels of CXCR5, and the binding of CXCL13 induces

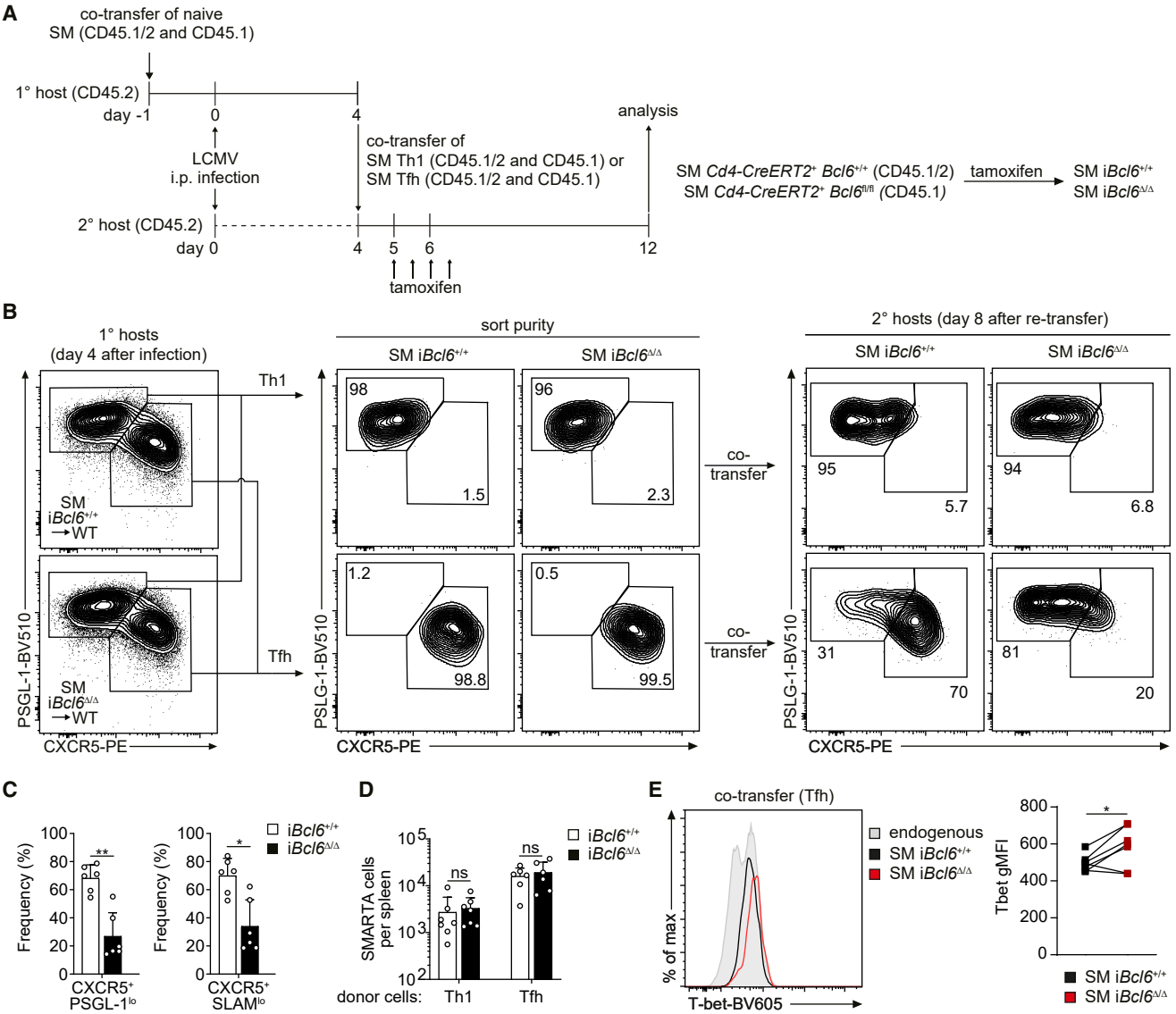

Figure 7. Bcl6 Prevents the Transdifferentiation of Tfh Cells into Th1 Cells during Acute Viral Infection

(A) Schematic representation of the experimental protocol for the analysis of the impact of induced CD4$^+$ T cell-specific ablation of *Bcl6* in SM cells when Tfh and Th1 cells were first generated through LCMV Armstrong infection and then transferred into pre-infected secondary hosts as depicted prior to *Bcl6* ablation.

(B) Flow cytometry of splenocytes from primary and secondary recipients, given adoptive transfers of SM cells. SM Tfh (CXCR5$^+$PSGL-1^{lo}) and SM Th1 (CXCR5$^-$PSGL-1^{hi}) cells were sorted from pooled spleens of primary recipient mice on day 4 after i.p. LCMV infection and retransferred into infection-matched secondary hosts (left panel). On day 12 after infection, the co-transferred Th1 (right panel, upper row) and Tfh cells (right panel, lower row) from SM *Cd4-CreERT2*$^+$ *Bcl6*$^{+/+}$ and SM *Cd4-CreERT2*$^+$ *Bcl6*$^{fl/fl}$ mice were quantified. The gate frequencies indicate the percentage of CXCR5$^-$PSGL-1^{hi} Th1 and CXCR5$^+$PSGL-1^{lo} Tfh cells.

(C and D) Quantification of the results depicted in (B); each symbol represents an individual mouse (n = 6–7).

(E) Flow cytometric analysis and quantification of T-bet expression in co-transferred SM Tfh cells analyzed on day 12 post-infection as in (B). "Endogenous" refers to polyclonal CD4$^+$ T cells of the infected secondary host mice.

*p < 0.05, **p < 0.01 two-tailed nonparametric Mann-Whitney test (C and D); paired t test (E); means ± SEMs in (C) and (D).

phosphatidylinositol 3-kinase (PI3K)-Akt signaling (Shi et al., 2018), which is essential for Tfh cells (Rolf et al., 2010). Although CXCR5 overexpression promotes enhanced GC localization (Shi et al., 2018), CXCR5-deficient CD4$^+$ T cells were shown to still enter GCs, however, with reduced LZ polarization (Greczmiel et al., 2017; Haynes et al., 2007). This was associated with impaired affinity maturation toward epitopes of LCMV (Greczmiel et al., 2017). Therefore, it is conceivable that CXCR5 on T cells functions to first efficiently recruit T cells to the GC and then confine T cell help and hence selection of high-affinity GC B cells to the LZ, without affecting T cell-intrinsic properties.

A possible disentanglement of the Tfh cell phenotype and CXCR5 expression was also recently suggested by the observation of peripheral PD-1^{hi}CXCR5^{-} Tfh-like cell populations with B cell helper abilities and Tfh cell marker expression patterns, for example, in the joints of rheumatoid arthritis patients and in tumors of cancer patients, although their ontogeny and function remain largely elusive (Gu-Trantien et al., 2017; Rao et al., 2017). The fact that many aspects of the GC B cell response were not altered by CD4^{+} T cell-specific *Cxcr5* ablation raises the question of how CXCR5^{-} Tfh cells manage to retain their GC localization. In our RNA-seq data, we could not find a compensatory upregulation of migratory modules upon the loss of CXCR5. A previous report showed that CXCR5 and S1PR2 have somewhat overlapping functions, and only CD4^{+} T cells deficient for both factors lost the capacity to enter GCs (Moriyama et al., 2014). Similar to control Tfh cells, *Cxcr5*-ablated Tfh cells in our experiments showed the continued expression of *S1pr2* and simultaneous downregulation of *Gpr183*, which encodes EBI2. Recently, Vanderleyden et al. (2020) showed that Tfr cells do not depend on CXCR5 to acquire and maintain GC localization, which complements our findings on the requirements of CD4^{+} T cell-expressed CXCR5 for Tfh cell and GC maintenance.

The slight increase in IgG1^{+} GC B cells that we observed in our inducible CD4^{+} T cell-specific *Cxcr5* deletion system stands in contrast to data from a study that used Cxcr5$^{-/-}$ CD4^{+} T cells and reported impaired class switching (Arnold et al., 2007). Class switching has recently been shown to be an early event that is initiated before GC formation, when activated T cells interact with primed B cells at the T:B zone border (Roco et al., 2019). If CD4^{+} T cells lack CXCR5 expression during this early phase, Tfh cell migration toward the B cell follicle may be less efficient and thus curtails class switching, whereas the deletion of CXCR5 at later stages could have less adverse effects.

The importance of Bcl6 expression for the induction of Tfh cell differentiation is well established (Hollister et al., 2013; Johnston et al., 2009; Nurieva et al., 2009; Poholek et al., 2010; Yu et al., 2009). One of the main functions of Bcl6 is the inhibition of the Tfh cell antagonist Blimp-1 (Johnston et al., 2009). As Tfh cells are completely absent in mice with a conditional knockout of *Bcl6* in CD4^{+} T cells, it was thus far not possible to easily address the role of Bcl6 beyond Tfh cell induction. Evidence for the function of Bcl6 in mature Tfh cells comes from chromatin immunoprecipitation sequencing (ChIP-seq) experiments that mapped the genomic occupancy at numerous genes relevant to Th1, Th2, and Th17 differentiation pathways (Hatzi et al., 2015; Liu et al., 2016), indicating a role for Bcl6 in preventing alternative cell fate programs. However, it has not been investigated before by detailed loss-of-function studies whether Bcl6 is required for the identity and function of fully matured Tfh cells. In our experiments, we found that GC Tfh cells, which express the highest levels of Bcl6, were particularly sensitive toward Bcl6 ablation, while Bcl6^{int} Tfh cells were only moderately affected. In GCs, Tfh cells must adapt to conditions such as hypoxia (Zhu et al., 2019), restricted localization within the LZ (Fuller et al., 1993; Haynes et al., 2007), and high concentrations of the antagonistic cytokine IL-2 (Papillion et al., 2019). High levels of Bcl6 may therefore be required to maintain GC localization by repressing several T cell zone migratory molecules such as CCR7 and PSGL-1 or chemotactic receptors responding to cues outside the GC, such as S1PR1 and EBI2 (Hatzi et al., 2015). More important, through the inhibition of other T helper cell programs, Bcl6 may enable Tfh cells to withstand non-Tfh cell cues, for example, IL-2 and interferon-γ (IFN-γ). Outside the GC, however, Tfh cells may not equally rely on Bcl6. Despite the collapse of the GC Tfh cell population upon *Bcl6* ablation, the frequencies of GC B cells were not similarly affected in our experiments, and a small but stable GC B cell population was maintained over time. CXCR5^{+}PD-1$^{int/lo}$ cells may be able to take over some of the functions of GC Tfh cells; however, these cells were not able to sustain normal frequencies of class-switched IgG1^{+} GC B cells.

Tfr cells share the expression of molecules that are normally associated with Tfh and Treg cells, as well as several molecular requirements for Tfh cell differentiation, such as co-stimulation and interactions with B cells (Chung et al., 2011; Linterman et al., 2011). Despite these striking similarities, we observed that Tfr cells were not equally affected by an induced loss of *Bcl6*. Moreover, when *Bcl6* was deleted at early time points after immunization, Tfr cell frequencies were largely unaltered. This is unexpected, as Tfr cells are unable to form in *Foxp3^{Cre} Bcl6$^{fl/fl}$* mice (Botta et al., 2017; Fu et al., 2018; Wu et al., 2016). Nevertheless, Bcl6 expression is lower in Tfr cells relative to Tfh cells (Chung et al., 2011) and may be dispensable after Tfr cell development. It is also possible that despite a normal phenotype, Tfr cells in induced *Bcl6*-deficient mice may be functionally impaired and contribute to the defects observed in the GC response. It was recently shown that in the absence of Tfr cells, Tfh cells adopt a cytotoxic phenotype and appear to induce apoptosis in GC B cells (Xie et al., 2019). This could be an additional explanation for the reduced GC B cell frequencies in our system.

Plasticity among CD4^{+} T helper cells is a widely accepted concept (DuPage and Bluestone, 2016; O'Shea and Paul, 2010), and several lines of evidence also point to the extensive plasticity of Tfh cells (Cannons et al., 2013). For example, *in vitro*-generated Tfh-like cells could be polarized to increase Th1, Th2, or Th17 cytokine expression (Lu et al., 2011). The loss of the miR-17-92 cluster in LCMV-specific SM cells resulted in the co-expression of a Th17 gene expression program that was layered on top of the Tfh cell program (Baumjohann et al., 2013a). Another study found that Tfh cells gave rise to pathogenic Th2 cells in an allergy model (Ballesteros-Tato et al., 2016). Our finding that *Bcl6* ablation in Tfh cells during LCMV Armstrong infection resulted in an increased plasticity toward Th1 cells expands the view of Bcl6 as a critical inhibitor of alternative T cell fates to already-established Tfh cells. The compatibility of Th1 and Tfh cell programs has been suggested by the co-expression of Bcl6 and T-bet in certain contexts, and Bcl6^{+} Tfh cells may also represent a transitional differentiation state or may serve as precursors for other effector cells (Sheikh et al., 2019; Baumjohann et al., 2011; Nakayamada et al., 2011; Oestreich et al., 2011; Weinstein et al., 2018; Yusuf et al., 2010). In our experiments, upon induced *Bcl6* ablation, LCMV-specific SM cells lost the characteristic surface marker expression of Tfh cells and downregulated Tfh cell-associated transcripts, including *Il6ra* and *Il6st*. The loss of the Tfh cell phenotype and the propensity to adopt a Th1 cell phenotype in

our temporally controlled *Bcl6* ablation system may be additionally explained by the findings of a recent study, in which IL-6 signaling during a viral infection was reported to shield Tfh cells from abundant IL-2 signals, which destabilize the Tfh cell phenotype (Papillion et al., 2019). Bcl6 expression in T cells has been previously shown to be required for the generation of Tfh cell-derived memory cells, in particular, of the central memory phenotype (Choi et al., 2013; Ichii et al., 2007; Kitano et al., 2011; Liu et al., 2012; Pepper et al., 2011). In this regard, our findings are in line with a study that showed a decrease in Tfh memory cells upon induced *Bcl6* deletion (Ise et al., 2014). Interestingly, the loss of Tfh cell identity that we observed following induced *Bcl6* ablation in $CD4^+$ T cells resembles the rapid loss of the Tfh cell phenotype that was also described when T-B cell interactions were disrupted by the blockade of CD40:CD40L and ICOSL:ICOS pathways during ongoing GC responses following protein immunization (Baumjohann et al., 2013b). This is relevant, since ICOS signaling promotes Bcl6 expression for Tfh cell differentiation (Choi et al., 2011), and ICOS is important for Tfh cell maintenance (Akiba et al., 2005; Weber et al., 2015). Our data indicate that when strong cues for other cell fate programs are present (e.g., predominant Th1-polarization during LCMV infection), Tfh cells are highly dependent on Bcl6 to prevent transdifferentiation into other T helper cell subsets, thus highlighting the plasticity of Tfh cells.

STAR★METHODS

Detailed methods are provided in the online version of this paper and include the following:

- KEY RESOURCES TABLE
- RESOURCE AVAILABILITY
  - Lead Contact
  - Materials Availability
  - Data and Code Availability
- EXPERIMENTAL MODEL AND SUBJECT DETAILS
- METHOD DETAILS
  - Immunizations, adoptive cell transfers, immunizations, infections, and tamoxifen treatment
  - Flow cytometry
  - Quantitative RT-PCR analysis
  - RNA-sequencing
- QUANTIFICATION AND STATISTICAL ANALYSIS

SUPPLEMENTAL INFORMATION

Supplemental Information can be found online at https://doi.org/10.1016/j.celrep.2020.108232.

ACKNOWLEDGMENTS

D.B. was supported by the Deutsche Forschungsgemeinschaft (DFG, German Research Foundation) under Emmy Noether Programme BA 5132/1-1 and BA 5132/1-2 (252623821), SFB 1054 Teilprojekt B12 (210592381), and Germany's Excellence Strategy EXC2151 (390873048), as well as by LMUexcellent. W.E. was supported by the DFG under SFB 1243 Teilprojekt A14. N.A.M. and B.M.B. were supported by the UK Biotechnology and Biological Sciences Research Council (grant nos. BB/F019762/1, BBS/E/D/10002071, and BBS/E/D/20002174). The authors would like to thank Helmut Blum and Stefan Krebs for the sequencing of libraries; Thomas Brocker, Dietmar Zehn, Yinshui Chang, and Lisa Rausch for help with LCMV titre determination; the BMC Core Facility Flow Cytometry of the LMU Munich for providing equipment; and Vigo Heissmeyer for discussions and comments on the manuscript.

AUTHOR CONTRIBUTIONS

D.A. designed, performed, and analyzed most of the experiments, interpreted the data, and wrote the manuscript. J.W.B. and W.E. provided critical tools and performed the RNA-seq analyses. F.D. performed the qPCR analyses. B.M.B. and N.A.M. provided the *Cxcr5*$^{fl/fl}$ mouse strain. T.B. provided the *Cd4-CreERT2* strain. D.B. conceived the project, designed the experiments, interpreted the data, wrote the manuscript, and provided the overall direction of the study. All of the authors read and approved the final version of the manuscript.

DECLARATION OF INTERESTS

The authors declare no competing interests.

Received: January 30, 2020
Revised: July 1, 2020
Accepted: September 15, 2020
Published: October 6, 2020

REFERENCES

Akiba, H., Takeda, K., Kojima, Y., Usui, Y., Harada, N., Yamazaki, T., Ma, J., Tezuka, K., Yagita, H., and Okumura, K. (2005). The role of ICOS in the CXCR5+ follicular B helper T cell maintenance in vivo. J. Immunol. *175*, 2340–2348.

Ansel, K.M., McHeyzer-Williams, L.J., Ngo, V.N., McHeyzer-Williams, M.G., and Cyster, J.G. (1999). In vivo-activated CD4 T cells upregulate CXC chemokine receptor 5 and reprogram their response to lymphoid chemokines. J. Exp. Med. *190*, 1123–1134.

Arnold, C.N., Campbell, D.J., Lipp, M., and Butcher, E.C. (2007). The germinal center response is impaired in the absence of T cell-expressed CXCR5. Eur. J. Immunol. *37*, 100–109.

Bagnoli, J.W., Ziegenhain, C., Janjic, A., Wange, L.E., Vieth, B., Parekh, S., Geuder, J., Hellmann, I., and Enard, W. (2018). Sensitive and powerful single-cell RNA sequencing using mcSCRB-seq. Nat. Commun. *9*, 2937.

Ballesteros-Tato, A., Randall, T.D., Lund, F.E., Spolski, R., Leonard, W.J., and León, B. (2016). T Follicular Helper Cell Plasticity Shapes Pathogenic T Helper 2 Cell-Mediated Immunity to Inhaled House Dust Mite. Immunity *44*, 259–273.

Baumjohann, D., and Ansel, K.M. (2015). Tracking early T follicular helper cell differentiation in vivo. Methods Mol. Biol. *1291*, 27–38.

Baumjohann, D., Okada, T., and Ansel, K.M. (2011). Cutting Edge: distinct waves of BCL6 expression during T follicular helper cell development. J. Immunol. *187*, 2089–2092.

Baumjohann, D., Kageyama, R., Clingan, J.M., Morar, M.M., Patel, S., de Kouchkovsky, D., Bannard, O., Bluestone, J.A., Matloubian, M., Ansel, K.M., and Jeker, L.T. (2013a). The microRNA cluster miR-17~92 promotes TFH cell differentiation and represses subset-inappropriate gene expression. Nat. Immunol. *14*, 840–848.

Baumjohann, D., Preite, S., Reboldi, A., Ronchi, F., Ansel, K.M., Lanzavecchia, A., and Sallusto, F. (2013b). Persistent antigen and germinal center B cells sustain T follicular helper cell responses and phenotype. Immunity *38*, 596–605.

Botta, D., Fuller, M.J., Marquez-Lago, T.T., Bachus, H., Bradley, J.E., Weinmann, A.S., Zajac, A.J., Randall, T.D., Lund, F.E., León, B., and Ballesteros-Tato, A. (2017). Dynamic regulation of T follicular regulatory cell responses by interleukin 2 during influenza infection. Nat. Immunol. *18*, 1249–1260.

Bradford, B.M., Reizis, B., and Mabbott, N.A. (2017). Oral Prion Disease Pathogenesis Is Impeded in the Specific Absence of CXCR5-Expressing Dendritic Cells. J. Virol. https://doi.org/10.1128/JVI.00124-17.

Breitfeld, D., Ohl, L., Kremmer, E., Ellwart, J., Sallusto, F., Lipp, M., and Förster, R. (2000). Follicular B helper T cells express CXC chemokine receptor 5, localize to B cell follicles, and support immunoglobulin production. J. Exp. Med. *192*, 1545–1552.

Cannons, J.L., Lu, K.T., and Schwartzberg, P.L. (2013). T follicular helper cell diversity and plasticity. Trends Immunol. *34*, 200–207.

Choi, Y.S., Kageyama, R., Eto, D., Escobar, T.C., Johnston, R.J., Monticelli, L., Lao, C., and Crotty, S. (2011). ICOS receptor instructs T follicular helper cell versus effector cell differentiation via induction of the transcriptional repressor Bcl6. Immunity *34*, 932–946.

Choi, Y.S., Yang, J.A., Yusuf, I., Johnston, R.J., Greenbaum, J., Peters, B., and Crotty, S. (2013). Bcl6 expressing follicular helper CD4 T cells are fate committed early and have the capacity to form memory. J. Immunol. *190*, 4014–4026.

Chung, Y., Tanaka, S., Chu, F., Nurieva, R.I., Martinez, G.J., Rawal, S., Wang, Y.H., Lim, H., Reynolds, J.M., Zhou, X.H., et al. (2011). Follicular regulatory T cells expressing Foxp3 and Bcl-6 suppress germinal center reactions. Nat. Med. *17*, 983–988.

Cossarizza, A., Chang, H.D., Radbruch, A., Acs, A., Adam, D., Adam-Klages, S., Agace, W.W., Aghaeepour, N., Akdis, M., Allez, M., et al. (2019). Guidelines for the use of flow cytometry and cell sorting in immunological studies (second edition). Eur. J. Immunol. *49*, 1457–1973.

Crotty, S. (2019). T Follicular Helper Cell Biology: A Decade of Discovery and Diseases. Immunity *50*, 1132–1148.

Deenick, E.K., Chan, A., Ma, C.S., Gatto, D., Schwartzberg, P.L., Brink, R., and Tangye, S.G. (2010). Follicular helper T cell differentiation requires continuous antigen presentation that is independent of unique B cell signaling. Immunity *33*, 241–253.

Dobin, A., Davis, C.A., Schlesinger, F., Drenkow, J., Zaleski, C., Jha, S., Batut, P., Chaisson, M., and Gingeras, T.R. (2013). STAR: ultrafast universal RNA-seq aligner. Bioinformatics *29*, 15–21.

DuPage, M., and Bluestone, J.A. (2016). Harnessing the plasticity of CD4(+) T cells to treat immune-mediated disease. Nat. Rev. Immunol. *16*, 149–163.

Fu, W., Liu, X., Lin, X., Feng, H., Sun, L., Li, S., Chen, H., Tang, H., Lu, L., Jin, W., and Dong, C. (2018). Deficiency in T follicular regulatory cells promotes autoimmunity. J. Exp. Med. *215*, 815–825.

Fuller, K.A., Kanagawa, O., and Nahm, M.H. (1993). T cells within germinal centers are specific for the immunizing antigen. J. Immunol. *151*, 4505–4512.

Goenka, R., Barnett, L.G., Silver, J.S., O'Neill, P.J., Hunter, C.A., Cancro, M.P., and Laufer, T.M. (2011). Cutting edge: dendritic cell-restricted antigen presentation initiates the follicular helper T cell program but cannot complete ultimate effector differentiation. J. Immunol. *187*, 1091–1095.

Greczmiel, U., Kräutler, N.J., Pedrioli, A., Bartsch, I., Agnellini, P., Bedenikovic, G., Harker, J., Richter, K., and Oxenius, A. (2017). Sustained T follicular helper cell response is essential for control of chronic viral infection. Sci. Immunol. *2*, eaam8686.

Gu-Trantien, C., Migliori, E., Buisseret, L., de Wind, A., Brohée, S., Garaud, S., Noël, G., Dang Chi, V.L., Lodewyckx, J.N., Naveaux, C., et al. (2017). CXCL13-producing TFH cells link immune suppression and adaptive memory in human breast cancer. JCI Insight *2*, e91487.

Hardtke, S., Ohl, L., and Förster, R. (2005). Balanced expression of CXCR5 and CCR7 on follicular T helper cells determines their transient positioning to lymph node follicles and is essential for efficient B-cell help. Blood *106*, 1924–1931.

Hatzi, K., Nance, J.P., Kroenke, M.A., Bothwell, M., Haddad, E.K., Melnick, A., and Crotty, S. (2015). BCL6 orchestrates Tfh cell differentiation via multiple distinct mechanisms. J. Exp. Med. *212*, 539–553.

Haynes, N.M., Allen, C.D., Lesley, R., Ansel, K.M., Killeen, N., and Cyster, J.G. (2007). Role of CXCR5 and CCR7 in follicular Th cell positioning and appearance of a programmed cell death gene-1high germinal center-associated subpopulation. J. Immunol. *179*, 5099–5108.

Hollister, K., Kusam, S., Wu, H., Clegg, N., Mondal, A., Sawant, D.V., and Dent, A.L. (2013). Insights into the role of Bcl6 in follicular Th cells using a new conditional mutant mouse model. J. Immunol. *191*, 3705–3711.

Ichii, H., Sakamoto, A., Arima, M., Hatano, M., Kuroda, Y., and Tokuhisa, T. (2007). Bcl6 is essential for the generation of long-term memory CD4+ T cells. Int. Immunol. *19*, 427–433.

Ise, W., Inoue, T., McLachlan, J.B., Kometani, K., Kubo, M., Okada, T., and Kurosaki, T. (2014). Memory B cells contribute to rapid Bcl6 expression by memory follicular helper T cells. Proc. Natl. Acad. Sci. USA *111*, 11792–11797.

Johnston, R.J., Poholek, A.C., DiToro, D., Yusuf, I., Eto, D., Barnett, B., Dent, A.L., Craft, J., and Crotty, S. (2009). Bcl6 and Blimp-1 are reciprocal and antagonistic regulators of T follicular helper cell differentiation. Science *325*, 1006–1010.

Junt, T., Fink, K., Förster, R., Senn, B., Lipp, M., Muramatsu, M., Zinkernagel, R.M., Ludewig, B., and Hengartner, H. (2005). CXCR5-dependent seeding of follicular niches by B and Th cells augments antiviral B cell responses. J. Immunol. *175*, 7109–7116.

Kitano, M., Moriyama, S., Ando, Y., Hikida, M., Mori, Y., Kurosaki, T., and Okada, T. (2011). Bcl6 protein expression shapes pre-germinal center B cell dynamics and follicular helper T cell heterogeneity. Immunity *34*, 961–972.

Linterman, M.A., Pierson, W., Lee, S.K., Kallies, A., Kawamoto, S., Rayner, T.F., Srivastava, M., Divekar, D.P., Beaton, L., Hogan, J.J., et al. (2011). Foxp3+ follicular regulatory T cells control the germinal center response. Nat. Med. *17*, 975–982.

Liu, X., Yan, X., Zhong, B., Nurieva, R.I., Wang, A., Wang, X., Martin-Orozco, N., Wang, Y., Chang, S.H., Esplugues, E., et al. (2012). Bcl6 expression specifies the T follicular helper cell program in vivo. J. Exp. Med. *209*, 1841–1852, S1–S24.

Liu, X., Lu, H., Chen, T., Nallaparaju, K.C., Yan, X., Tanaka, S., Ichiyama, K., Zhang, X., Zhang, L., Wen, X., et al. (2016). Genome-wide Analysis Identifies Bcl6-Controlled Regulatory Networks during T Follicular Helper Cell Differentiation. Cell Rep. *14*, 1735–1747.

Love, M.I., Huber, W., and Anders, S. (2014). Moderated estimation of fold change and dispersion for RNA-seq data with DESeq2. Genome Biol. *15*, 550.

Lu, K.T., Kanno, Y., Cannons, J.L., Handon, R., Bible, P., Elkahloun, A.G., Anderson, S.M., Wei, L., Sun, H., O'Shea, J.J., and Schwartzberg, P.L. (2011). Functional and epigenetic studies reveal multistep differentiation and plasticity of in vitro-generated and in vivo-derived follicular T helper cells. Immunity *35*, 622–632.

Maul, J., Alterauge, D., and Baumjohann, D. (2019). MicroRNA-mediated regulation of T follicular helper and T follicular regulatory cell identity. Immunol. Rev. *288*, 97–111.

Moriyama, S., Takahashi, N., Green, J.A., Hori, S., Kubo, M., Cyster, J.G., and Okada, T. (2014). Sphingosine-1-phosphate receptor 2 is critical for follicular helper T cell retention in germinal centers. J. Exp. Med. *211*, 1297–1305.

Moschovakis, G.L., Bubke, A., Friedrichsen, M., Falk, C.S., Feederle, R., and Förster, R. (2017). T cell specific Cxcr5 deficiency prevents rheumatoid arthritis. Sci. Rep. *7*, 8933.

Nakayamada, S., Kanno, Y., Takahashi, H., Jankovic, D., Lu, K.T., Johnson, T.A., Sun, H.W., Vahedi, G., Hakim, O., Handon, R., et al. (2011). Early Th1 cell differentiation is marked by a Tfh cell-like transition. Immunity *35*, 919–931.

Nurieva, R.I., Chung, Y., Martinez, G.J., Yang, X.O., Tanaka, S., Matskevitch, T.D., Wang, Y.H., and Dong, C. (2009). Bcl6 mediates the development of T follicular helper cells. Science *325*, 1001–1005.

O'Shea, J.J., and Paul, W.E. (2010). Mechanisms underlying lineage commitment and plasticity of helper CD4+ T cells. Science *327*, 1098–1102.

Oestreich, K.J., Huang, A.C., and Weinmann, A.S. (2011). The lineage-defining factors T-bet and Bcl-6 collaborate to regulate Th1 gene expression patterns. J. Exp. Med. *208*, 1001–1013.

Okada, T., Miller, M.J., Parker, I., Krummel, M.F., Neighbors, M., Hartley, S.B., O'Garra, A., Cahalan, M.D., and Cyster, J.G. (2005). Antigen-engaged B cells undergo chemotaxis toward the T zone and form motile conjugates with helper T cells. PLOS Biol. *3*, e150.

Oxenius, A., Bachmann, M.F., Zinkernagel, R.M., and Hengartner, H. (1998). Virus-specific MHC-class II-restricted TCR-transgenic mice: effects on

humoral and cellular immune responses after viral infection. Eur. J. Immunol. *28*, 390–400.

Papillion, A., Powell, M.D., Chisolm, D.A., Bachus, H., Fuller, M.J., Weinmann, A.S., Villarino, A., O'Shea, J.J., León, B., Oestreich, K.J., and Ballesteros-Tato, A. (2019). Inhibition of IL-2 responsiveness by IL-6 is required for the generation of GC-T_{FH} cells. Sci. Immunol. *4*, eaaw7636.

Parekh, S., Ziegenhain, C., Vieth, B., Enard, W., and Hellmann, I. (2018). zUMIs - a fast and flexible pipeline to process RNA sequencing data with UMIs. Gigascience *7*, giy059.

Pepper, M., Pagán, A.J., Igyártó, B.Z., Taylor, J.J., and Jenkins, M.K. (2011). Opposing signals from the Bcl6 transcription factor and the interleukin-2 receptor generate T helper 1 central and effector memory cells. Immunity *35*, 583–595.

Poholek, A.C., Hansen, K., Hernandez, S.G., Eto, D., Chandele, A., Weinstein, J.S., Dong, X., Odegard, J.M., Kaech, S.M., Dent, A.L., et al. (2010). In vivo regulation of Bcl6 and T follicular helper cell development. J. Immunol. *185*, 313–326.

Qi, H. (2016). T follicular helper cells in space-time. Nat. Rev. Immunol. *16*, 612–625.

Qin, L., Waseem, T.C., Sahoo, A., Bieerkehazhi, S., Zhou, H., Galkina, E.V., and Nurieva, R. (2018). Insights Into the Molecular Mechanisms of T Follicular Helper-Mediated Immunity and Pathology. Front. Immunol. *9*, 1884.

Rao, D.A., Gurish, M.F., Marshall, J.L., Slowikowski, K., Fonseka, C.Y., Liu, Y., Donlin, L.T., Henderson, L.A., Wei, K., Mizoguchi, F., et al. (2017). Pathologically expanded peripheral T helper cell subset drives B cells in rheumatoid arthritis. Nature *542*, 110–114.

Roco, J.A., Mesin, L., Binder, S.C., Nefzger, C., Gonzalez-Figueroa, P., Canete, P.F., Ellyard, J., Shen, Q., Robert, P.A., Cappello, J., et al. (2019). Class-Switch Recombination Occurs Infrequently in Germinal Centers. Immunity *51*, 337–350.e7.

Rolf, J., Bell, S.E., Kovesdi, D., Janas, M.L., Soond, D.R., Webb, L.M., Santinelli, S., Saunders, T., Hebeis, B., Killeen, N., et al. (2010). Phosphoinositide 3-kinase activity in T cells regulates the magnitude of the germinal center reaction. J. Immunol. *185*, 4042–4052.

Schaerli, P., Willimann, K., Lang, A.B., Lipp, M., Loetscher, P., and Moser, B. (2000). CXC chemokine receptor 5 expression defines follicular homing T cells with B cell helper function. J. Exp. Med. *192*, 1553–1562.

Sheikh, A.A., Cooper, L., Feng, M., Souza-Fonseca-Guimaraes, F., Lafouresse, F., Duckworth, B.C., Huntington, N.D., Moon, J.J., Pellegrini, M., Nutt, S.L., et al. (2019). Context-Dependent Role for T-bet in T Follicular Helper Differentiation and Germinal Center Function following Viral Infection. Cell Rep *28*, 1758–1772.

Shi, J., Hou, S., Fang, Q., Liu, X., Liu, X., and Qi, H. (2018). PD-1 Controls Follicular T Helper Cell Positioning and Function. Immunity *49*, 264–274.e4.

Sledzińska, A., Hemmers, S., Mair, F., Gorka, O., Ruland, J., Fairbairn, L., Nissler, A., Müller, W., Waisman, A., Becher, B., and Buch, T. (2013). TGF-β signalling is required for $CD4^+$ T cell homeostasis but dispensable for regulatory T cell function. PLOS Biol. *11*, e1001674.

Vanderleyden, I., Fra-Bido, S.C., Innocentin, S., Stebegg, M., Okkenhaug, H., Evans-Bailey, N., Pierson, W., Denton, A.E., and Linterman, M.A. (2020). Follicular Regulatory T Cells Can Access the Germinal Center Independently of CXCR5. Cell Rep. *30*, 611–619.e4.

Vinuesa, C.G., Linterman, M.A., Yu, D., and MacLennan, I.C. (2016). Follicular Helper T Cells. Annu. Rev. Immunol. *34*, 335–368.

Weber, J.P., Fuhrmann, F., Feist, R.K., Lahmann, A., Al Baz, M.S., Gentz, L.J., Vu Van, D., Mages, H.W., Haftmann, C., Riedel, R., et al. (2015). ICOS maintains the T follicular helper cell phenotype by down-regulating Krüppel-like factor 2. J. Exp. Med. *212*, 217–233.

Weinstein, J.S., Laidlaw, B.J., Lu, Y., Wang, J.K., Schulz, V.P., Li, N., Herman, E.I., Kaech, S.M., Gallagher, P.G., and Craft, J. (2018). STAT4 and T-bet control follicular helper T cell development in viral infections. J. Exp. Med. *215*, 337–355.

Wickham, H. (2016). ggplot2: Elegant Graphics for Data Analysis (Springer-Verlag New York).

Wu, H., Chen, Y., Liu, H., Xu, L.L., Teuscher, P., Wang, S., Lu, S., and Dent, A.L. (2016). Follicular regulatory T cells repress cytokine production by follicular helper T cells and optimize IgG responses in mice. Eur. J. Immunol. *46*, 1152–1161.

Xie, M.M., Fang, S., Chen, Q., Liu, H., Wan, J., and Dent, A.L. (2019). Follicular regulatory T cells inhibit the development of granzyme B-expressing follicular helper T cells. JCI Insight *4*, e128076.

Yu, D., Rao, S., Tsai, L.M., Lee, S.K., He, Y., Sutcliffe, E.L., Srivastava, M., Linterman, M., Zheng, L., Simpson, N., et al. (2009). The transcriptional repressor Bcl-6 directs T follicular helper cell lineage commitment. Immunity *31*, 457–468.

Yusuf, I., Kageyama, R., Monticelli, L., Johnston, R.J., Ditoro, D., Hansen, K., Barnett, B., and Crotty, S. (2010). Germinal center T follicular helper cell IL-4 production is dependent on signaling lymphocytic activation molecule receptor (CD150). J. Immunol. *185*, 190–202.

Zeitrag, J., Alterauge, D., Dahlstrom, F., and Baumjohann, D. (2020). Gene dose matters: Considerations for the use of inducible CD4-CreER(T2) mouse lines. Eur. J. Immunol. *50*, 603–605.

Zhu, Y., Zhao, Y., Zou, L., Zhang, D., Aki, D., and Liu, Y.C. (2019). The E3 ligase VHL promotes follicular helper T cell differentiation via glycolytic-epigenetic control. J. Exp. Med. *216*, 1664–1681.

STAR★METHODS

KEY RESOURCES TABLE

REAGENT or RESOURCE	SOURCE	IDENTIFIER
Antibodies		
anti-CD4-PB	BioLegend	Cat# 100531; RRID: AB_493374
anti-CD4-BV510	BioLegend	Cat#:100559 RRID: AB_2562608
anti-CD4-BUV395	BD Biosciences	Cat# 740208; RRID: AB_2734761
anti-CD45.1-APC	BioLegend	Cat# 110713; RRID: AB_313502
anti-CD45.1-BV510	BioLegend	Cat# 110741; RRID: AB_2563378
anti-CD45.1-FITC	BioLegend	Cat# 110706; RRID: AB_313495
anti-CD45.2-V450	BD Biosciences	Cat# 560697; RRID: AB_1727495
anti-CD45.2-FITC	Thermo Fisher Scientific	Cat# 11-0454-85; RRID: AB_465062
anti-CD44-AF700	BioLegend	Cat# 103026; RRID: AB_493713
anti-CXCR5-Biotin (clone L138D7)	BioLegend	Cat# 145509; RRID: AB_2562125
anti-PD1-BV711 (clone 29F.1A12)	BioLegend	Cat# 135231; RRID: AB_2566158
anti-PD1-PE-eF610 (clone J43)	Thermo Fisher Scientific	Cat# 61-9985-82; RRID: AB_2574688
anti-SLAM-BV650	BioLegend	Cat# 115931; RRID: AB_2562402
anti-PSGL-1-BV510	BD Bioscience	Cat# 563448; RRID: AB_2738211
anti-GITR-BV711	BD Bioscience	Cat# 563390; RRID: AB_2738176
anti-CD19-BV605	BioLegend	Cat# 115540; RRID: AB_2563067
anti-CD19-BV510	BioLegend	Cat# 115546; RRID: AB_2562137
anti-CD19-AF488	BioLegend	Cat# 115521; RRID: AB_389307
anti-IgD-BV786 (clone 11-26c.2a)	BD Biosciences	Cat# 563618; RRID: AB_2738322
anti-IgD-eF450 (clone 11-26c (11-26))	Thermo Fisher Scientifics	Cat# 48-5993-82; RRID: AB_1272202
anti-Fas-PE-Cy7	BD Biosciences	Cat# 557653; RRID: AB_396768
anti-Fas-BV605	BD Biosciences	Cat# 740367; RRID: AB_2740099
anti-IgG1-BV421	BD Biosciences	Cat# 562580; RRID: AB_2737664
anti-IgG1-FITC	BD Biosciences	Cat# 553443; RRID: AB_394862
anti-Foxp3-PE-Cy7	Thermo Fisher Scientific	Cat# 25-5773-82; RRID: AB_891552
anti-Foxp3-AF488	Thermo Fisher Scientific	Cat# 53-5773-82; RRID: AB_763537
anti-Bcl6-PE (clone K112-91)	BD Biosciences	Cat# 561522; RRID: AB_10717126
anti-Bcl6-AF647 (clone K112-91)	BD Biosciences	Cat# 561525; RRID: AB_10898007
anti-T-bet-PE-Cy7	Thermo Fisher Scientific	Cat# 25-5825-82; RRID: AB_11042699
anti-T-bet-BV605	BioLegend	Cat# 644817; RRID: AB_11219388
Bacterial and Virus Strains		
LCMV Armstrong	Zehn Laboratory	Generated in house
Chemicals, Peptides, and Recombinant Proteins		
7-AAD	Thermo Fisher Scientific	Cat# 00-6993-50
2-mercaptoethanol	Sigma-Aldrich	Cat# M6250
Imject Alum	Thermo Fisher Scientific	Cat# 77161
Corn oil	Sigma-Aldrich	Cat# C8267
Exonuclease I	NEB	Cat# M0293
Fixable Viability Dye eFluor 780	Thermo Fisher Scientific	Cat# 65-0865-14
Fluoromount G	Thermo Fisher Scientific	Cat# 00-4958-02
Guanidine hydrochloride	Sigma-Aldrich	Cat# G3272
Maxima H Minus Reverse Transcriptase	Thermo Fisher Scientific	Cat# EP0753

(*Continued on next page*)

Continued

REAGENT or RESOURCE	SOURCE	IDENTIFIER
NP_{24}-KLH or 4-hydroxy-3-nitrophenylacetyl conjugated to keyhole limpet hemocyanin	Biosearch Technologies	Cat# N-5060
Proteinase K solution	Ambion	Cat# AM2546
Streptavidin-APC	BioLegend	Cat# 405207
Streptavidin-PE	BioLegend	Cat# 405204
Tamoxifen	Sigma-Aldrich	Cat# T5648
Taq Polymerase	NEB	Cat# M0273S
Terra PCR Direct Polymerase Mix	Takara Bio	Cat# 639287
UltraPure DNase/RNase-Free Distilled Water	Thermo Fisher Scientific	Cat# 10977-049
Critical Commercial Assays		
$CD4^+$ T cell Isolation Kit, mouse	Miltenyi Biotech	Cat# 130-104-454
CleanNGS	CleanNA	Cat# CNGS-0050
EasySep Mouse Naive $CD4^+$ T cell Isolation Kit	STEMCELL Technologies	Cat# 19765
Foxp3 / Transcription Factor Staining buffer set	Thermo Fisher Scientific	Cat# 00-5523-00
High Sensitivity DNA Analysis Kits	Agilent Technologies	Cat# 5067-4626
Nextera XT DNA Sample Preparation Kit	Illumina	Cat# FC-131-1024 and Cat# FC-131-1001
SensiFAST Probe No-ROX One-Step Kit	Bioline	Cat# BIO-76001
Deposited Data		
RNA-Sequencing data	This work	GEO: GSE142229
Experimental Models: Organisms/Strains		
Bcl6$^{fl/fl}$ (*Bcl6*$^{tm1.1Dent}$)	The Jackson Laboratory	JAX #023727
C57BL/6	Charles River or Janvier Laboratories	n/a
CD45.1 (*Ptprc*^{a} *Pepc*^{b}/BoyJ)	The Jackson Laboratory	JAX #002014
Cd4-CreERT2 knock-in (*CD4*$^{tm1(CreERt2)ThBu}$)	Sledzińska et al., 2013	n/a
Cxcr5$^{fl/fl}$ (*Cxcr5*$^{tm1.Namt}$)	Bradford et al., 2017	n/a
Rosa26$^{fl\text{-}Stop\text{-}fl\text{-}eYFP}$ (*Gt(ROSA) 26Sor*$^{tm1(eYFP)Cos}$)	The Jackson Laboratory	JAX #006148
SMARTA (Tg(TcrLCMV)Aox)	Oxenius et al., 1998	n/a
B6.Cg-Cd4$^{tm1(cre/ERT2)Thbu}$-*Cxcr5*$^{tm1.Namt}$	This work	n/a
B6.Cg-Tg(TcrLCMV)Aox-Ptprc^a Pepc^b-Cd4$^{tm1(cre/ERT2)Thbu}$	This work	n/a
B6.Cg-Tg(TcrLCMV)Aox-Ptprc^a Pepc^b-Cd4$^{tm1(cre/ERT2)Thbu}$-Cxcr5$^{tm1.1Namt}$	This work	n/a
B6.Cg-Cd4$^{tm1(cre/ERT2)Thbu}$-Gt(ROSA) 26Sor$^{tm1(EYFP)Cos}$	This work	n/a
B6.Cg-Cd4$^{tm1(cre/ERT2)Thbu}$-*Bcl6*$^{tm1.1Dent}$-Gt(ROSA)26Sor$^{tm1(EYFP)Cos}$	This work	n/a
B6.Cg-Tg(TcrLCMV)Aox-Ptprc^a Pepc^b-Cd4$^{tm1(cre/ERT2)Thbu}$-Gt(ROSA) 26Sor$^{tm1(EYFP)Cos}$	This work	n/a
B6.Cg-Tg(TcrLCMV)Aox-Ptprc^a Pepc^b-Cd4$^{tm1(cre/ERT2)Thbu}$- *Bcl6*$^{tm1.1Dent}$-Gt(ROSA) 26Sor$^{tm1(EYFP)Cos}$	This work	n/a
Oligonucleotides		
PrimeTime Assay Bcl6	IDTDNA	Mm.PT.58.1178966; FAM
PrimeTime Assay Actb	IDTDNA	Assay ID: Mm.PT.58.33257376.gs; HEX

(*Continued on next page*)

Continued

REAGENT or RESOURCE	SOURCE	IDENTIFIER
Bcl6 gDNA F (ACCACTGACCCAGAGGATTA)	IDTDNA	Custom
Bcl6 gDNA R (GCTTCAAATCCCAGCAAAGG)	IDTDNA	Custom
CXCR5 gDNA F (ACATCCTGGTGCTGGTAATC)	IDTDNA	Custom
CXCR5 gDNA R (ACTAAGAGAAGGTCGGCTACT)	IDTDNA	Custom
Software and Algorithms		
FlowJo software	https://www.flowjo.com/	RRID:SCR_008520
GraphPad Prism 8	https://www.graphpad.com/	RRID:SCR_002798
Cowplot	Love et al., 2014	RRID:SCR_018081
Ggplot2	Wickham, 2016	RRID:SCR_014601
ImageJ	https://imagej.net/Welcome	RRID:SCR_003070
Light Cycler 480 SW 1.5.1	Roche	RRID:SCR_012155
STAR 2.6.0a	https://github.com/alexdobin/STAR	RRID:SCR_015899
zUMIS	https://github.com/sdparekh/zUMIs	RRID:SCR_016139

RESOURCE AVAILABILITY

Lead Contact

Further information and requests for resources and reagents should be directed to and will be fulfilled by the Lead Contact, Dirk Baumjohann (dirk.baumjohann@uni-bonn.de).

Materials Availability

This study generated several mouse strains by intercrossing various commercially and non-commercially available mouse strains. There are restrictions to the availability of the generated strains as some of the original strains were obtained under material transfer agreement that do not permit redistribution of these strains without prior permission of the strain owner.

Data and Code Availability

Source transcriptomic data are available through GEO: GSE142229. Other source data are available from the Lead Contact upon reasonable request.

EXPERIMENTAL MODEL AND SUBJECT DETAILS

Cd4-CreERT2 knock-in (*C57BL/6-CD4*$^{tm1(CreERt2)ThBu}$) mice (Sledzińska et al., 2013) and *Cxcr5*$^{fl/fl}$ (*Cxcr5*$^{tm1.Namt}$) mice (Bradford et al., 2017) have been described previously. *Bcl6*$^{fl/fl}$ (*Bcl6*$^{tm1.1Dent}$, stock number 023727) and *Rosa26*$^{fl\text{-}Stop\text{-}fl\text{-}YFP}$ (*Gt(ROSA)26Sor*$^{tm1(EYFP)Cos}$, stock number 006148) mice were purchased from The Jackson Laboratory. For adoptive transfer experiments, compound mouse lines were further intercrossed with LCMV GP_{61-80} peptide-specific SMARTA TCR-tg mice (Oxenius et al., 1998) and congenic CD45.1 alleles. Wild-type C57BL/6 mice were purchased from Charles River or Janvier Labs. All Mice were housed under specific pathogen free conditions in individually ventilated cages and all animal experiments were performed in accordance with European Regulation and Federal Law and approved by the Regierung von Oberbayern. All mice used for experiments were used at 8-12 weeks of age. Experimental groups were sex and age-matched. To better reveal the dynamic range of the gene ablation effects, our approved animal protocol containing limited numbers of experimental animals focused on testing a wide range of different tamoxifen application and analysis time points as well as independently reproducing the results in two different experimental systems with sufficient numbers of animals, instead of performing extensive repetition experiments for only a few time points.

METHOD DETAILS

Immunizations, adoptive cell transfers, immunizations, infections, and tamoxifen treatment

For immunizations, 4-hydroxy-3-nitrophenylacetyl conjugated to keyhole limpet hemocyanin (NP_{24}-KLH, Biosearch Technologies) dissolved in PBS was mixed 1:1 with alum (Imject Alum, Thermo Scientific) and rotated for 45 min at room temperature prior to

immunization. Mice were anesthetized by isoflurane inhalation and injected s.c. with 10μg NP-KLH into the hock of each hind limb using an insulin syringe (BD Biosciences). Adoptive cell transfers of SMARTA cells into wild-type hosts were performed as previously described (Baumjohann et al., 2013a). In brief, naive CD4$^+$ T cells were isolated from spleens and LNs of SMARTA mice through negative selection using the EasySep Mouse Naive CD4 T cell isolation kit (StemCell Technologies). For most experiments, 1x10^4 naive SMARTA cells were adoptively transferred in PBS into wild-type recipients by tail vein injection, followed by i.p. injection of 2x10^5 pfu LCMV Armstrong. Tamoxifen-induced ablation experiments were performed with *Cd4-CreERT2* knock-in mice as previously described (Zeitrag et al., 2020). In brief, tamoxifen (1g, Sigma-Aldrich) was dissolved in 100% Ethanol (1ml). 29ml corn oil (Sigma-Aldrich) were added and the mixture was incubated in a water bath at 56°C until the solid tamoxifen was fully dissolved. Aliquots of the 33.3 mg/ml stock solution were stored at −20°C until further use. Mice received a dose of 5 mg tamoxifen in 150 μl volume by intragastric gavage twice daily on two consecutive days (either day 3 and 4 or day 6 and 7 after immunization). For the retransfer experiment, 0.5x10^6 naive SMARTA cells were adoptively transferred into wild-type mice one day prior to infection with 1x10^6 pfu LCMV Armstrong. Tfh and Th1 cells derived from the transferred CD45.1/2 *Cd4-CreERT2*$^+$*Bcl6*$^{+/+}$ and CD45.1/1 *Cd4-CreERT2*$^+$*iBcl6*$^{fl/fl}$ SMARTA cells were sorted as CXCR5$^+$PSGL-1^{lo} and CXCR5$^-$PSGL-1^{hi}, respectively, into PBS + 2% FCS, washed, and counted. 2x10^4 Th1 or Tfh cells from both genotypes were then co-transferred into infection-matched secondary wild-type hosts. Recipients were gavaged with tamoxifen one and two days after the re-transfer.

Flow cytometry

General guidelines for the use of flow cytometry and cell sorting in immunological studies were followed (Cossarizza et al., 2019). Single-cell suspensions from spleen or peripheral lymph nodes were prepared by mincing the tissue between the frosted ends of glass slides. Dead cells were excluded with 7-AAD (eBioscience/Thermo Fisher) for surface maker analyses or with the fixable viability dye eFluor 780 (eBioscience/Thermo Fisher) for intracellular analyses. Before staining of surface/intracellular molecules, Fc receptors were blocked by preincubation of cells with anti-CD16/32 (clone 93; Biolegend) and 1% mouse/rat serum (StemCell Technologies). The following antibodies were used for analyses by flow cytometry: CD4 (RM4-5, BD Biosciences, BioLegend), CD45.2 (104, BD Biosciences, eBioscience), CD86 (GL1, BD Biosciences, Biolegend); CD19 (6D5), CD44 (IM7), CD45.1 (A20), PD-1 (29F.1A12), SLAM (TC15-12F12.2) (all Biolegend); Fas (Jo2), GITR (DTA-1), IgG1 (A85-1), PSLG-1 (2PH1) (all BD Bioscience); CXCR4 (2B11), PD-1 (J43), IgD (11-26c) (all eBioscience). CXCR5 was stained with biotinylated anti-CXCR5 (clone L138D7 from Biolegend) for 30min on ice, followed by washing and incubation with streptavidin conjugated to APC or PE (Biolegend) for 15min on ice (Baumjohann and Ansel, 2015). Intracellular transcription factor stainings were performed with the Foxp3 Staining Set from eBioscience using the following fluorophore-coupled mAbs: Bcl6 (K112-91, BD Biosciences), T-bet (4B10, BioLegend) and Foxp3 (FJK-16 s, eBioscience). NP-PE (4-Hydroxy-3-nitrophenylacetyl hapten conjugated to phycoerythrin) was purchased from Biosearch Technologies (conjugation ratio 28:1). Samples were acquired on a three-laser BD FACS Canto II or a 5-laser BD LSRFortessa using BD FACSDiva software. Cell sorting was performed on a BD FACSAriaFusion. Data were analyzed with FlowJo software (Treestar).

Quantitative RT-PCR analysis

RT-qPCR was used to quantify deletion efficiency of *Bcl6* genomic DNA und mRNA. 200-500 CXCR5$^+$ PD-1$^+$ cells were sorted into a 96-well qPCR plate (Roche Diagnostics) containing 5 μl lysis buffer consisting of a 1:500 dilution of Phusion HF buffer (New England Biolabs) in nuclease free water (Thermo Fisher). Cellular components were removed by proteinase K (Ambion) digest for 10 minutes at 55°C, followed by desiccation at 95°C for 10 minutes without a seal to reduce the volume and inactivate proteinase K. RNA was subsequently transcribed into cDNA using the SensiFast One-Step Real-Time RT-PCR kit (Bioline). The expression of *Bcl6* mRNA was measured by multiplexed qRT-PCR using PrimeTime gene expression probes (IDTDNA) for *Bcl6* (Mm.PT.58.11789661; FAM) and the housekeeper *Actb* (Mm.PT.58.33257376.gs; HEX). For the quantification of *Bcl6* gDNA, the reverse transcriptase step was omitted and custom PrimeTime probes (IDTDNA) for genomic *Bcl6* (F: ACCACTGACCCAGAGGATTAFAM; R: GCTTCAAATCCCAG CAAAGG; FAM) and the control gene *Cxcr5* (F: AACATCCTGGTGCTGGTAATC; R: ACTAAGAGAAGGTCGGCTACT; HEX) were used. The expression was measured on a Light Cycler 480II (Roche) device with the Light Cycler 480 SW 1.5.1 software.

RNA-sequencing

For RNA-seq analysis, 1,000-2,000 Tfh or non-Tfh cells were sorted into a 96-well plate containing 50 μl lysis buffer using a FACSAriaFusion cell sorter (BD Biosciences). The lysis buffer consisted of 5 M Guanidine hydrochloride (Sigma-Aldrich), 1% 2-mercaptoethanol (Sigma-Aldrich) and a 1:500 dilution of Phusion HF buffer (New England Biolabs). After sorting the cells were briefly centrifuged and immediately frozen on dry ice. cDNA was then generated using a modified version of the single cell RNA-seq protocol mcSCRB (Bagnoli et al., 2018). cDNA was tagmented with the Nextera XT DNA Library Prep Kit (Illumina) using 0.8 ng as input. Libraries were paired-end sequenced on high output flow cells of an Illumina HiSeq 1500 instrument at LAFUGA Genomics of LMU Munich's Gene Center. Sixteen bases were sequenced with the first read to obtain cellular and molecular barcodes and 50 bases were sequenced in the second read into the cDNA fragment. An additional 8 bp bases were sequenced to obtain the i7 barcode. All raw fastq data were processed with zUMIs (Parekh et al., 2018) and mapped to the mouse genome (mm10) using STAR 2.6.0a (Dobin et al., 2013). Gene annotations were obtained from Ensembl (GRCm38.75). Samples were identified via the i7 and Cellular Barcode or only the i7 barcode, with initial phred score filtering allowing 2 or 1 bases below 20, respectively. UMI phred filtering allowed 2 bases below 20. After initial data processing, generated count matrices were loaded into R. We filtered out sparsely detected

genes via UMI per genes and detection abundance (> 1 UMI) over all samples. Afterwards libraries were normalized with DESeq2 (Love et al., 2014). Hierarchical clustering for marker gene expression was performed using Complex Heatmaps. Differentially expressed genes were called with DESeq2. All plotting was performed using ggplot2 and cowplot.

QUANTIFICATION AND STATISTICAL ANALYSIS

Statistical analyses were performed with Prism 8 (GraphPad) and are specified in each corresponding figure legend.